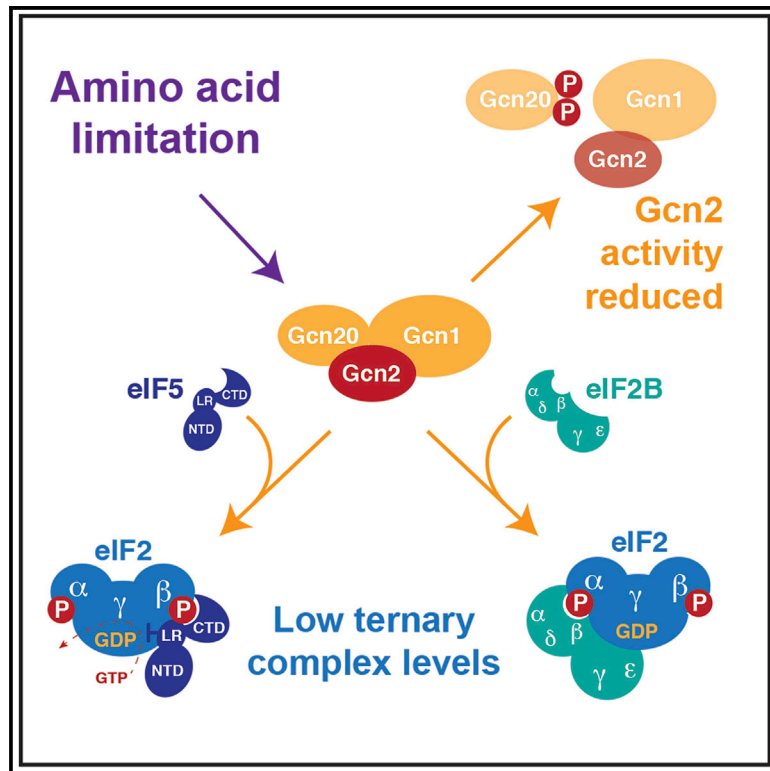


Global phosphoproteomics pinpoints uncharted Gcn2-mediated mechanisms of translational control

Graphical abstract



Authors

Ladislav Dokládál, Michael Stumpe, Benjamin Pillet, ..., Dieter Kressler, Jörn Dengjel, Claudio De Virgilio

Correspondence

claudio.devirgilio@unifr.ch

In brief

The Gcn2 kinase mediates cellular adaptations to amino acid limitation through the translational control of gene expression that is primarily executed by eIF2 α phosphorylation. Here, Dokládál et al. show that Gcn2 targets auxiliary, physiologically relevant effectors, including eIF2 β and Gcn20, to fine-tune translational control in response to amino acid starvation.

Highlights

- Global phosphoproteomics identifies hitherto elusive physiological Gcn2 targets
- Gcn2 phosphorylates eIF2 β to promote the GDI function of eIF5 toward eIF2-GDP
- This restricts eIF2 ternary complex recycling in amino-acid-starved cells
- Gcn2 engages in a negative autoregulatory feedback loop by targeting Gcn20



Article

Global phosphoproteomics pinpoints uncharted Gcn2-mediated mechanisms of translational control

Ladislav Dokládal,¹ Michael Stumpe,¹ Benjamin Pillet,¹ Zehan Hu,¹ Guillermo Miguel Garcia Osuna,¹ Dieter Kressler,¹ Jörn Dengjel,¹ and Claudio De Virgilio^{1,2,*}

¹Department of Biology, University of Fribourg, CH-1700 Fribourg, Switzerland

²Lead contact

*Correspondence: claudio.devirgilio@unifr.ch

<https://doi.org/10.1016/j.molcel.2021.02.037>

SUMMARY

The conserved Gcn2 protein kinase mediates cellular adaptations to amino acid limitation through translational control of gene expression that is exclusively executed by phosphorylation of the α -subunit of the eukaryotic translation initiation factor 2 (eIF2 α). Using quantitative phosphoproteomics, however, we discovered that Gcn2 targets auxiliary effectors to modulate translation. Accordingly, Gcn2 also phosphorylates the β -subunit of the trimeric eIF2 G protein complex to promote its association with eIF5, which prevents spontaneous nucleotide exchange on eIF2 and thereby restricts the recycling of the initiator methionyl-tRNA-bound eIF2-GDP ternary complex in amino-acid-starved cells. This mechanism contributes to the inhibition of translation initiation in parallel to the sequestration of the nucleotide exchange factor eIF2B by phosphorylated eIF2 α . Gcn2 further phosphorylates Gcn20 to antagonize, in an inhibitory feedback loop, the formation of the Gcn2-stimulatory Gcn1-Gcn20 complex. Thus, Gcn2 plays a substantially more intricate role in controlling translation initiation than hitherto appreciated.

INTRODUCTION

Adaptation to changes in extracellular amino acid levels critically define the growth and survival of cells. Eukaryotes use two primordial signaling pathways that allow them to sense and respond to fluctuating levels of amino acids, namely the general control nonderepressible 2 (Gcn2) and the target of rapamycin complex 1 (TORC1) pathways that are activated by the absence and presence, respectively, of amino acids (Albert and Hall, 2015; Hinnebusch, 2005; Wolfson and Sabatini, 2017). Gcn2 senses and is activated by uncharged tRNAs that accumulate when amino acids become limiting (Dong et al., 2000; Zhu et al., 1996). Active Gcn2 phosphorylates the α -subunit of the eukaryotic translation initiation factor eIF2 (a G protein complex) to inhibit general translation initiation and activate translational derepression of specific mRNAs (Dever et al., 1992; Hinnebusch, 1996). Mechanistically, guanosine triphosphate (GTP)-bound eIF2 fulfills an essential function for protein synthesis by delivering the initiator methionyl-tRNA (as eIF2-GTP-tRNA^{Met} ternary complex [TC]) to the 40S ribosome, which then scans and selects the translation initiation codon. Gcn2-mediated phosphorylation of eIF2 α (eIF2 α P), however, limits the levels of GTP-bound eIF2 and consequently those of TCs that are available for translation initiation by converting eIF2 from a substrate to an inhibitor of its guanine nucleotide exchange factor (GEF) eIF2B. While this globally dampens translation, it also stimulates the translation of specific mRNAs such as *GCN4* in yeast and

ATF4 in mammals, which code for transcription factors that induce the expression of a large set of genes involved in the cellular adaptation to amino acid limitation (Hinnebusch, 2005; Kilberg et al., 2009). The respective translational stimulation is based on a particular re-initiation mechanism that allows pre-initiation complexes to bypass upstream open reading frames (uORFs) in the 5' untranslated regions (UTRs) of *GCN4* and *ATF4* mRNAs and reach the main ORF (Mueller and Hinnebusch, 1986; Vattam and Wek, 2004).

The TORC1 kinase is a master regulator of cell growth that couples environmental and nutritional cues to downstream effectors that oppositely control anabolic (e.g., protein synthesis) and catabolic (e.g., macroautophagy) processes (Albert and Hall, 2015; Laplante and Sabatini, 2012). Amino acids signal to TORC1 through various sensory modules and upstream regulators that converge on the conserved heterodimeric Rag guanosine triphosphatases (GTPases) consisting of RagA (or RagB) and RagC (or RagD) in higher eukaryotes and Gtr1 and Gtr2 in yeast (Binda et al., 2009; Kim et al., 2008; Sancak et al., 2008). Amino acid abundance promotes a configuration of the Rag GTPases that activates TORC1 (i.e., RagA/B/Gtr1 GTP and RagC/D/Gtr2 guanosine diphosphate [GDP] loaded), while amino acid starvation converts the Rag GTPases into their opposite loading state that inactivates TORC1 (Binda et al., 2009; Demetriades et al., 2014; Kim et al., 2008; Sancak et al., 2008). Interestingly, the TORC1 and Gcn2 signaling pathways are wired to each other through a feedback regulatory loop in which (1)



TORC1 inhibits Gcn2 (by preventing the dephosphorylation of Gcn2-pSer⁵⁷⁷ and thus reducing the affinity of Gcn2 for uncharged tRNAs) and (2) Gcn2 inhibits TORC1 (possibly through phosphorylation of its subunit Kog1) (Cherkasova and Hinnebusch, 2003; Yuan et al., 2017).

Based on global phosphoproteomic studies, we show here that the Gcn2 kinase targets other proteins, in addition to eIF2 α , that have hitherto remained elusive. Specifically, Gcn2 phosphorylates the β -subunit of eIF2 (eIF2 β or Sui3) to promote its association with the translation initiation factor eIF5 (Tif5). This event is physiologically relevant as Ser to Ala mutation of the Gcn2 target residue in eIF2 β compromises its proper association with eIF5 and partially reduces the capacity of cells to inhibit translation initiation when treated with rapamycin or starved for amino acids, without changing their eIF2 α P levels. These data elucidate a missing mechanistic aspect of a model in which amino acid starvation-induced eIF2-eIF5 complex formation limits the GDP release by and spontaneous nucleotide exchange on eIF2 to restrict TC recycling in parallel to eIF2 α P-mediated sequestration of eIF2B (Jennings and Pavitt, 2010). In addition to eIF2 β , Gcn2 also phosphorylates Gcn20. This phosphorylation weakens the Gcn1-Gcn20 complex formation and hence the capacity of this complex to activate Gcn2 by uncharged tRNAs *in vivo* (Vazquez de Aldana et al., 1995). Thus, our data also highlight the existence of a feedback inhibition loop that modulates Gcn2 activity itself.

RESULTS AND DISCUSSION

Global phosphoproteomics identifies hitherto elusive Gcn2 targets

The only known *bona fide* target of the protein kinase Gcn2 in yeast is Ser⁵² of the eukaryotic translation initiation factor eIF2 α (Sui2) (Dever et al., 1992). To identify additional Gcn2 target proteins, we performed a set of stable isotope labeling by amino acids in cell culture (SILAC)-based quantitative phosphoproteomic experiments (Figure 1A). Briefly, we compared wild-type (WT) cells to *gcn2 Δ* and *sui2^{S52A}* cells (n = 3), all treated or not treated with rapamycin, which has previously been shown to stimulate eIF2 α phosphorylation by Gcn2 (Cherkasova and Hinnebusch, 2003). These experiments led to the identification of 35,401 phosphosites, 32,110 of which could be quantified (Figure 1B). A total of 27,596 sites could be localized to specific amino acid residues (localization probability ≥ 0.75 ; Olsen et al., 2006) and were normalized to changes in protein abundance. These sites were used for further analyses (Table S1). The rationale for choosing these strains and experimental conditions relied on both positive and negative selection criteria. By comparing WT to *gcn2 Δ* cells, both treated with rapamycin, Gcn2 target sites should be upregulated in WT cells (Figure 1C, positive selection I). In addition, sites should respond positively to rapamycin treatment in WT cells compared to non-treated WT cells based on our recently published rapamycin-sensitive phosphoproteome (Hu et al., 2019; positive selection II). Sui2 phosphorylation by Gcn2 leads to the translational upregulation of the transcription factor Gcn4, which regulates the expression of 500–1,000 different target genes (Figure 1C) (Jia et al., 2000; Natarajan et al., 2001). By comparing rapamycin-treated WT and *sui2^{S52A}* cells, which

are defective in Gcn4 upregulation, we further aimed at discriminating proximal Gcn2 effectors from distal effectors that act downstream of Gcn4. All of the phosphosites that were identified as upregulated in WT compared to *sui2^{S52A}* cells were therefore removed from our list of potential direct Gcn2 targets (Figure 1C, negative selection I). Finally, we also compared rapamycin-treated *gcn2 Δ* to non-treated *gcn2 Δ* cells and also removed all of the sites that were rapamycin sensitive in this setting (n = 3, negative selection II). These stringent filter criteria led to a shortlist of 18 of 27,596 phosphosites, including the known target site Sui2-Ser⁵², that were significantly regulated and fulfilled the criteria of being excellent candidates for Gcn2 target sites (Figure 1D; p < 0.05, >2-fold change, ≥ 4 data points per site). The amino acid residues surrounding these 18 phosphosites were used to identify a potential Gcn2 phosphorylation site motif (Figure 1E). Accordingly, Gcn2 seems to prefer negatively charged amino acids at positions -2 (glutamic acid: E), $+1$ (E), and $+5$ (aspartate: D), and positively charged ones at positions $+2$ (lysine: K) and $+4$ (K and arginine: R). The 16 target proteins carrying significantly regulated sites were further analyzed for known protein-protein interactions using STRING DB (Szklarczyk et al., 2019), which allowed us to generate a protein interaction network consisting of Gcn2 and 9 target proteins (Figure 1F). Interestingly, 8 of these 9 proteins are implicated in protein synthesis. Also, a Gene Ontology (GO) term analysis of target proteins led to a significant enrichment of terms related to mRNA translation and translation initiation (Figure 1G). Our unbiased approach confirms the general assumption that Gcn2 has a rather limited target profile, which is dedicated mainly to the control of protein synthesis and pinpoints 15 potential Gcn2 kinase substrates that have hitherto remained elusive.

Gcn2 has been suggested to directly phosphorylate the raptor N-terminal conserved (RNC) domain in Kog1 to mediate TORC1 inhibition in leucine-starved cells (Yuan et al., 2017). Interestingly, using less stringent criteria than that above in analyzing our phosphoproteome dataset, we also identified one residue in Kog1 (i.e., Ser⁴⁸⁷ within the RNC domain) that appeared to be regulated in a Gcn2-dependent manner in rapamycin-treated cells (Table S1). The phosphorylation status of this residue, however, was similarly affected in *gcn2 Δ* and *Sui2^{S52A}*-expressing cells, which indicates that it is likely controlled by distal Gcn2 effectors (at least in rapamycin-treated cells) and explains why it was not retained in our list of potential proximal Gcn2 targets (Figure 1D). To examine whether Gcn2 may control TORC1 via distal effectors in leucine-starved cells, we asked whether loss of Gcn2 and of its downstream effector Gcn4 would cause a similar defect in TORC1 inactivation upon leucine starvation. This was indeed the case (Figure S1). Thus, we deem it likely that Gcn2 inhibits TORC1 *in vivo* indirectly through the Gcn4-mediated expression of a protein that inhibits TORC1 signaling, perhaps as in mammalian cells, where Gcn2 sustains mTORC1 inhibition via ATF4-mediated expression of Sestrin2, a leucine sensor that inhibits mTORC1 signaling through GATOR1 (Ye et al., 2015).

Sui3-Ser⁸⁰ and Gcn20-Thr⁹⁴/Ser⁹⁵ are physiologically relevant Gcn2 target residues

To select some of the newly identified potential Gcn2 target residues for further analysis, we applied an additional criterion for

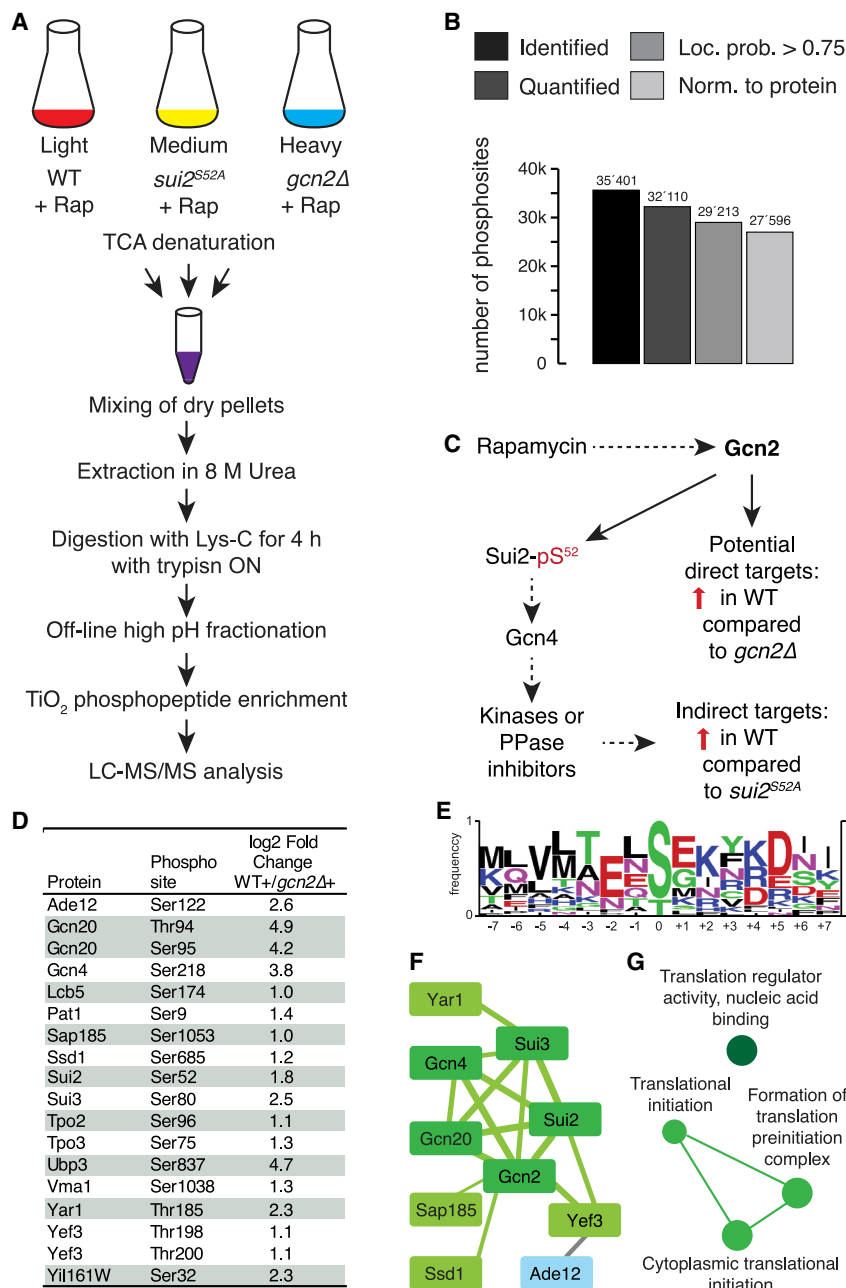


Figure 1. Quantitative phosphoproteomic analyses for the identification of potential Gcn2 target sites

(A) Quantitative MS-based phosphoproteomics workflow. Yeast cells were labeled with light (Lys0, Arg0), medium (Lys4, Arg6), or heavy (Lys8, Arg10) amino acid variants, and phosphopeptides were enriched and analyzed as outlined. Cells were treated or not treated with 200 ng mL⁻¹ rapamycin for 30 min. A minimum of 3 biological replicate analyses per condition were performed.

(B) Combined numbers of identified and quantified phosphosites. Data filtering steps are indicated.

(C) Rationale for choosing the indicated yeast strains and stimulation conditions.

(D) List of potential direct Gcn2 target sites fulfilling the 4 selection criteria (see text for details). All of the sites were minimally 2-fold regulated (log₂ ≥ 1) comparing WT cells to *gcn2Δ* cells treated with rapamycin (+). See also Figure S1.

(E) Motif analysis of shortlisted potential Gcn2 target sites.

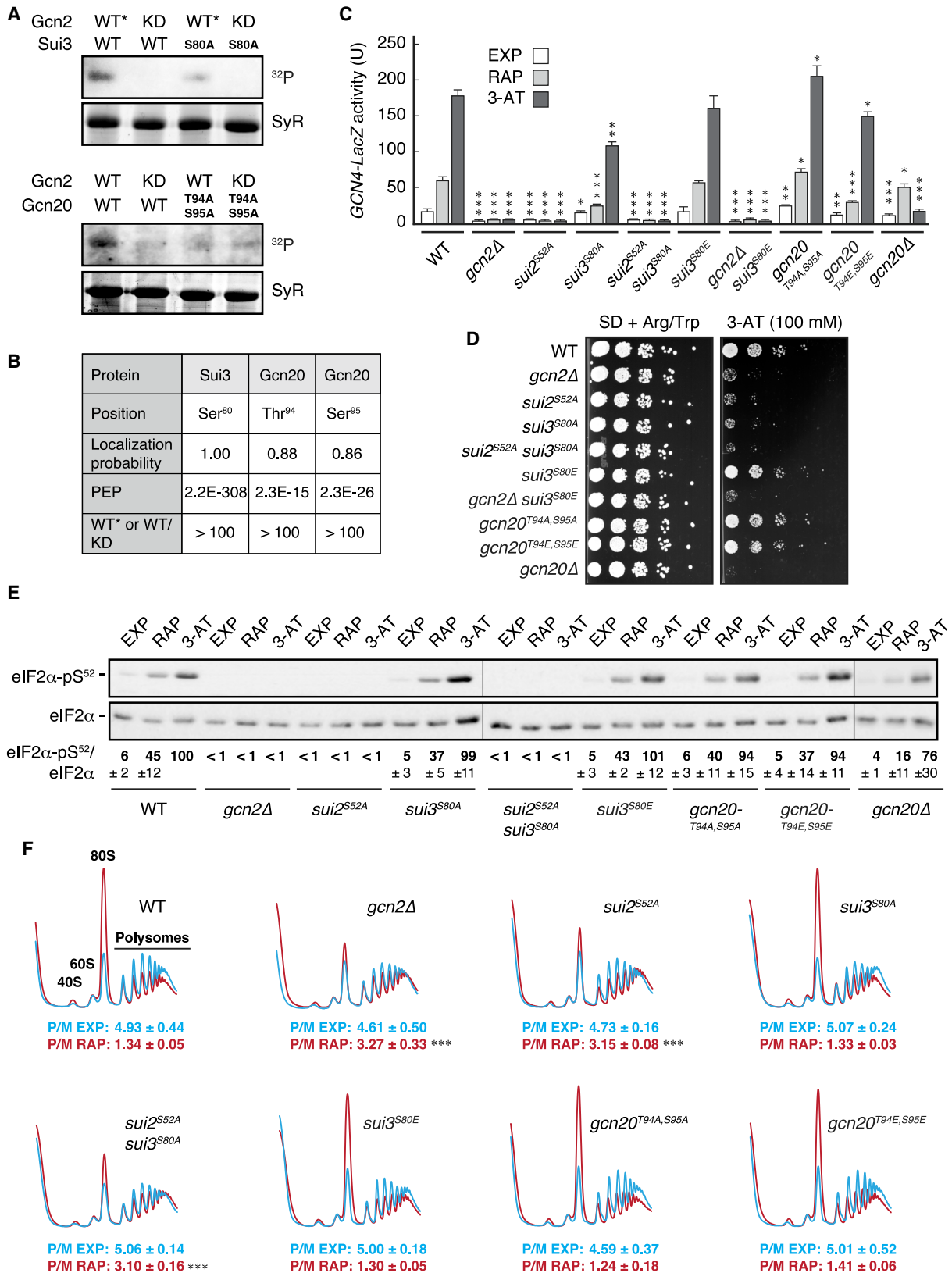
(F) Protein-protein interactions of potential Gcn2 targets. Interactions according to STRING DB (Szklarczyk et al., 2019). Thickness of edges indicate confidence of data support. Proteins colored in green are linked to protein synthesis.

(G) GO term enrichment analysis of shortlisted potential Gcn2 target proteins.

filtering our data, namely, that positive hits should also be significantly regulated by Gcn2 in leucine-starved cells. To this end, we acquired an independent phosphoproteome dataset (in duplicate) using leucine-starved WT and *gcn2Δ* cells (Table S2). The respective results prompted us to further examine the role of Sui3-Ser⁸⁰ and Gcn20-Ser⁹⁵ (together with Gcn20-Thr⁹⁴), as these residues were, like Sui2-Ser⁵² (eIF2 α -Ser⁵²), among the ones that were most robustly phosphorylated in a Gcn2-dependent manner in both rapamycin-treated (Figure 1D; Table S1) and leucine-starved (>2-fold in both leucine starvation experiments; Table S2) cells. To assess whether Gcn2 may directly phosphorylate Sui3 and/or Gcn20, we submitted the

respective recombinant proteins to *in vitro* kinase assays. Gratifyingly, a hyperactive Gcn2^{F842L} variant and Gcn2, but not kinase-dead Gcn2^{KD} (Gcn2^{K628R}), were able to phosphorylate Sui3 and Gcn20, respectively, *in vitro* (Figure 2A). Because the Gcn2 variants were virtually unable to phosphorylate recombinant Sui3^{S80A} or Gcn20^{T94A,S95A} (Figure 2A), we inferred that the respective amino acids represent the most critical Gcn2-modified residues. Mass spectrometry (MS) analyses of *in vitro* Gcn2-phosphorylated Sui3 and Gcn20 confirmed that Sui3-Ser⁸⁰, Gcn20-Thr⁹⁴, and Gcn20-Ser⁹⁵ were specifically phosphorylated by Gcn2 and not by Gcn2^{KD} (Figure 2B). Kinetic *in vitro* analyses further indicated that yeast Gcn2^{F842L} and/or human GCN2 phosphorylate Sui3 and Gcn20 with affinities comparable to or even higher than those for Sui2 (Figure S2). Combined with our *in vivo* analyses, these data establish Sui3 and Gcn20 as direct Gcn2 targets.

Sui3, the β -subunit of eIF2, and Gcn20, which dimerizes with Gcn1 to activate Gcn2, are both implicated in translation initiation (Hinnebusch, 2005). To study the role, if any, of Gcn2-mediated phosphorylation of Sui3 and Gcn20 for translation initiation *in vivo*, we next measured the impact of Ser/Thr to Ala (A) or phosphomimetic Glu (E) mutations of the relevant Gcn2 target residues on *GCN4-LacZ* expression, a sensitive reporter for the activity of translation initiation factors (Hinnebusch, 2005).



(legend on next page)

As previously reported (Cherkasova and Hinnebusch, 2003), *GCN4-LacZ* expression was very low in exponentially growing WT cells and became strongly derepressed, in a Gcn2- and eIF2 α -dependent manner, following either rapamycin treatment or histidine starvation (imposed by the addition of 3-amino-1,2,4-triazole [3-AT]; Figure 2C). Interestingly, *sui3*^{S80A} cells were partially but significantly compromised for both rapamycin- and 3-AT-induced derepression of *GCN4-LacZ* (by >58% and >38%, respectively), which was not the case for rapamycin- and 3-AT-treated *sui3*^{S80E} cells. Defective derepression of *GCN4* translation is associated with 3-AT-sensitive cell growth. Consistent with this, *sui3*^{S80A} and the other mutants that exhibited a *GCN4-LacZ* derepression defect (i.e., *gcn2* Δ , *sui2*^{S52A}, and *sui2*^{S52A} *sui3*^{S80A}), but not *sui3*^{S80E}, were sensitive to 3-AT (Figures 2D and S3). We considered it possible, therefore, that phosphorylation of Ser⁸⁰ in Sui3 contributes to the global inhibition of translation initiation in rapamycin-treated or -starved cells by promoting eIF2 α levels. However, in contrast to *gcn2* Δ and *sui2*^{S52A} cells, *sui3*^{S80A} cells were not impaired in their capacity to phosphorylate eIF2 α or to inhibit general translation initiation (as assayed by determining the polysome:monosome ratios [P:M] from polysome profiles) in 3-AT- or rapamycin-treated cells (Figures 2E and 2F). Gcn2-mediated phosphorylation of Sui3 therefore contributes to *GCN4* expression through another mechanism (see below).

The combined mutation of Thr⁹⁴ and Ser⁹⁵ in Gcn2 to either Ala or Glu yielded the Gcn2^{T94A,S95A} or Gcn2^{T94E,S95E} variants, which significantly enhanced (by 34%) and reduced (by 33%), respectively, the expression of *GCN4-LacZ* in exponentially growing cells. Similarly, Gcn2^{T94A,S95A} and Gcn2^{T94E,S95E} variants also significantly enhanced (by >14%) and reduced (by >17%), respectively, the expression of *GCN4-LacZ* in rapamycin- and 3-AT-treated cells (Figure 2C). Neither *gcn2* allele altered the 3-AT sensitivity or the relative eIF2 α P levels (Figures 2D and 2E). The latter matched our expectations because the loss of Gcn2 only moderately affected eIF2 α P under the same conditions (Figure 2E), although it rendered cells 3-AT sensitive and weakly reduced *GCN4-LacZ* expression in rapamycin-treated and more substantially in 3-AT-treated cells (Figures 2C, 2D, and S3). Notably, in a similar experiment, eIF2 α P levels

were previously also found to be only mildly reduced in *gcn2* Δ cells (Vazquez de Aldana et al., 1995). Nevertheless, our polysome profile analyses indicated that Gcn2^{T94A,S95A}-expressing cells exhibited moderately reduced global translation initiation levels in the exponential growth phase and after rapamycin treatment (i.e., 10.6% and 7.6% lower P:M ratios, respectively), while Gcn2^{T94E,S95E}-expressing cells exhibited normal translation initiation levels in the exponential growth phase, but slightly higher global translation initiation levels in rapamycin-treated cells (i.e., a 8.6% higher P:M ratio) (Figure 2F). Thus, although our polysome profile analyses of Gcn2^{T94A,S95A}- and Gcn2^{T94E,S95E}-expressing cells are not significantly different from those of WT cells, they are congruent with our *GCN4-LacZ* expression analyses in that they indicate a moderate, opposite effect of the non-phosphorylatable and phosphomimetic Gcn2 variants on translation initiation. In summary, Sui3-Ser⁸⁰ and Gcn2-Thr⁹⁴/Ser⁹⁵ are *bona fide* Gcn2 target residues that are relevant for the proper translational control of *GCN4* mRNA *in vivo*, although their contribution to the downregulation of global translation initiation by Gcn2 is subtle.

Gcn2 promotes eIF2-eIF5 association through phosphorylation of Sui3-Ser⁸⁰

Interestingly, Ser⁸⁰ lies between 2 of the 3 lysine-rich boxes in the N terminus of Sui3, which mediate binding to the aromatic and acidic residue-rich bipartite motifs in the C-terminal domain of both eIF5 (Tif5) and the catalytic eIF2B ϵ -subunit Gcd6 (Asano et al., 1999). We therefore speculated that the Gcn2-mediated phosphorylation of this residue may alter the affinity of Sui3 for Tif5 and/or Gcd6. This was the case for the Sui3-Tif5 interaction: a Sui3⁶⁸⁻⁸⁹ peptide (including Ser⁸⁰ and the lysine-rich box 3; Asano et al., 1999), when phosphorylated at Ser⁸⁰ (pS⁸⁰-Sui3⁶⁸⁻⁸⁹), bound 15.2-fold more tightly to recombinant Tif5 than a respective non-phosphorylated (Sui3⁶⁸⁻⁸⁹) control peptide when assayed *in vitro* using fluorescence spectroscopy (Figure 3A). Recombinant Gcd6, in contrast, exhibited a lower affinity for both pS⁸⁰-Sui3⁶⁸⁻⁸⁹ and Sui3⁶⁸⁻⁸⁹ (Figure 3B). In essence, our *in vivo* co-immunoprecipitation analyses validated these results. Accordingly, 3-AT treatment, which stimulates the activity of Gcn2, strongly reinforced (as also reported earlier; Jennings

Figure 2. Sui3-Ser⁸⁰ and Gcn2-Thr⁹⁴/Ser⁹⁵ are physiologically relevant Gcn2 target residues

(A and B) *In vitro* phosphorylation of Sui3-Ser⁸⁰ and Gcn2-Thr⁹⁴/Ser⁹⁵ by Gcn2. Recombinant His₆-Sui3 (Sui3) and His₆-Gcn2 (Gcn2) variants were subjected to *in vitro* kinase assays using hyperactive Gcn2^{F842L} (WT*), WT Gcn2 (WT), or kinase-dead Gcn2^{KD} purified from 3-AT-treated yeast cells. Representative autoradiographs (³²P) and SYPRO Ruby (SyR)-stained gels are shown in (A). Similar kinase assays were also carried out with cold ATP and analyzed by MS. The phosphorylation levels of the indicated residues (position) were compared between samples treated with Gcn2^{F842L} (WT*; for Sui3) or Gcn2 (WT; for Gcn2) and the ones treated with Gcn2^{KD} (KD) (B). Localization probabilities and posterior error probabilities (PEP) are indicated. See also Figure S2.

(C) *GCN4-LacZ* derepression in *sui2*, *sui3*, *gcn2*, and *gcn2* Δ mutants. Exponentially growing cells (EXP; genotypes indicated) expressing a plasmid-encoded *GCN4-LacZ* reporter were treated for 4 h with 200 ng mL⁻¹ rapamycin (RAP) or 40 mM 3-AT. β -Galactosidase activities (n = 3; \pm SD) were measured in whole-cell extracts and expressed as Miller units (U).

(D) 3-AT sensitivity of *sui2*, *sui3*, *gcn2*, and *gcn2* Δ mutants. Exponentially growing strains were spotted (10-fold serial dilutions) and grown for 3 days at 30°C on SD + Arg/Trp or 100 mM 3-AT-containing plates. See also Figure S3.

(E) eIF2 α P analyses. EXP (genotypes indicated) were treated for 30 min with 200 ng mL⁻¹ RAP or 20 mM 3-AT and analyzed for eIF2 α P levels using anti-eIF2 α -pSer⁵² and anti-eIF2 α antibodies. The mean ratios of eIF2 α -pS⁵²/eIF2 α (n = 3; \pm SD) were normalized to the one of 3-AT-treated wild-type (WT) cells (set to 100%).

(F) Polysome profile analyses. EXP were treated for 30 min with 200 ng mL⁻¹ RAP and used for polysome profile analyses. The positions corresponding to the 40S and 60S subunits, the 80S monosomes, and polysomal ribosomes are indicated in the WT profile. The ratios (n = 3; \pm SD) between polysome and 80S fractions are indicated (P:M) for EXP (light blue) and RAP-treated (red) cells.

Unpaired Student's t tests were used to determine significant differences in (C) and (F) when compared to the respective WT control (*p \leq 0.05; **p \leq 0.001; ***p \leq 0.0001).

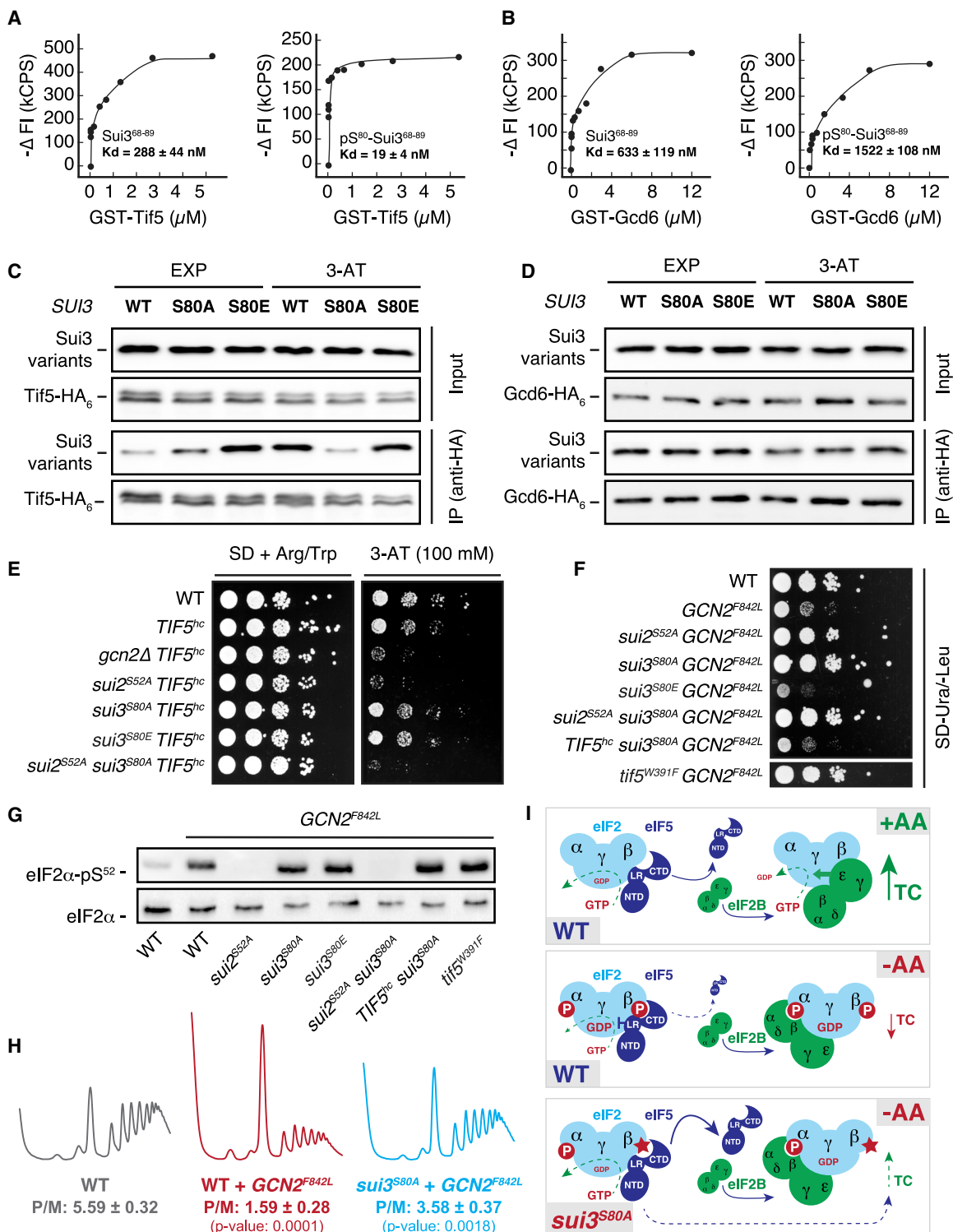


Figure 3. Gcn2 promotes eIF2-eIF5 association through phosphorylation of eIF2β/Sui3 on Ser⁸⁰

(A and B) Phosphorylation of Ser⁸⁰ in Sui3⁶⁸⁻⁸⁹ influences its affinity for eIF5/Tif5 and Gcd6 *in vitro*. The binding affinities of recombinant GST-Tif5 and GST-Gcd6 for the fluorescein-labeled Sui3⁶⁸⁻⁸⁹ peptide, phosphorylated (right panels) or not (left panels) on Ser⁸⁰, were determined by fluorescence quenching. Three independent measurements were performed at room temperature, with standard deviations being <7% (for A) or <15% (for B) for each presented data point. The concentration of Sui3⁶⁸⁻⁸⁹ peptide was 500 nM. Dissociation constants (K_D; n = 3; ±SD) were calculated using nonlinear asymmetric sigmoidal regressions. ΔFI, relative difference in fluorescence intensity; kCPS, kilo counts per second.

(legend continued on next page)

and Pavitt, 2010) the otherwise weak association between Sui3 and Tif5 observed in exponentially growing cells (Figure 3C). Sui3^{S80A}, in contrast, remained weakly associated with Tif5, even after 3-AT treatment, while the phosphomimetic Sui3^{S80E} variant was able to constitutively and tightly bind Tif5 in exponentially growing cells, notably to the same extent as in 3-AT-treated cells (Figure 3C). In further agreement with our *in vitro* assays, all 3 Sui3 variants exhibited similar affinities for Gcd6 in exponentially growing and 3-AT-treated cells, with overall slightly reduced associations between Sui3 variants and Gcd6 under the latter condition (Figure 3D). Together with our genetic data, our biochemical data therefore establish a model in which Gcn2 phosphorylates eIF2 β /Sui3 at Ser⁸⁰ to stimulate its association with eIF5/Tif5.

Notably, Tif5 plays a dual role as a GTPase activating protein (GAP) for the eIF2-GTP-tRNA^{Met} TC during mRNA start site selection and as a GDP dissociation inhibitor (GDI) for eIF2-GDP (Jennings and Pavitt, 2010). Due to the role of Tif5 in start site selection, certain mutant alleles of Tif5, like mutant alleles of its binding partner Sui3, can engage in non-AUG start codon recognition (a phenotype coined suppressor of initiation codon mutation [Sui⁻]). Depending on the type of mutation, these alleles can constitutively derepress (Gcd⁻ phenotype; which is not the case for *sui3*^{S80E} or *sui3*^{S80E} *gcn2* Δ cells; Figures 2C, 2D, and S3) or prevent the derepression (Gcn⁻ phenotype) of *GCN4* mRNA translation (Antony and Alone, 2017; Thakur et al., 2019). To evaluate whether the Sui3^{S80A/E} mutations may affect *GCN4* mRNA translation by affecting start codon selectivity, we measured the expression of *HIS4-LacZ* reporters containing either an AUG or UUG start codon (Donahue and Cigan, 1988). Expression of the Sui3^{S80A/E} alleles, like expression of the Sui2^{S52A} allele alone or combined with Sui3^{S80A}, and like the loss of Gcn2, had little impact on the UUG:AUG ratio in this assay, while the expression of the Tif5^{G31R} allele significantly increased (>5-fold) the UUG:AUG ratio, as previously reported (Antony and Alone, 2017; Thakur et al., 2019) (Figure S4). Thus, the mutation

of Ser⁸⁰ in Sui3 does not affect near cognate start codon recognition on the *HIS4-lacZ* reporter.

The second function of Tif5—its GDI activity—is specifically important in amino acid-starved cells to prevent spontaneous nucleotide exchange on eIF2, and thus to restrict its recycling to TC. This occurs in parallel to the inhibition of the eIF2B ϵ -mediated nucleotide exchange through the tethering of eIF2B $\alpha\beta\delta$ to eIF2 α P (Krishnamoorthy et al., 2001; Mohammad-Qureshi et al., 2007). The enhanced GDI function of Tif5 toward eIF2-GDP in amino acid-starved cells is eIF2 α P independent, requires guiding by a C-terminal domain in eIF2 β /Sui3, and relies on the stimulation of eIF2-Tif5 complex formation by a yet-unidentified mechanism (Jennings et al., 2016; Jennings and Pavitt, 2010). In this context, our data provide a mechanistic explanation for these earlier observations; the eIF2-Tif5 association is triggered by Gcn2-dependent phosphorylation of Sui3-Ser⁸⁰, which enables it to more efficiently recruit Tif5. Based on this model, we predicted that Sui3^{S80A}-expressing cells would be less susceptible to the Tif5-mediated GDI action and therefore exhibit higher TC levels that translate into lower *GCN4-LacZ* expression and increased 3-AT sensitivity. In agreement with this model, overproduction of Tif5 (from a high-copy plasmid; *TIF5*^{hc}), which we assumed would restore the formation of Sui3^{S80A}-Tif5 complexes by mass action, suppressed the 3-AT sensitivity of *sui3*^{S80A} cells, but not the sensitivity of eIF2 α P-deficient cells (i.e., *gcn2* Δ , *sui2*^{S52A}, and *sui2*^{S52A} *sui3*^{S80A}; Figures 2D, 3E, and S3). To evaluate the importance of Sui3-Ser⁸⁰ phosphorylation for the inhibition of translation in general, we also used a hyperactive Gcn2^{F842L} allele that severely reduces growth rates by inhibiting global translation initiation (Qiu et al., 2002). Intriguingly, the mutation of Ser⁸⁰ to Ala in Sui3, but not Ser⁸⁰ to Glu, suppressed the growth inhibition imposed by the expression of Gcn2^{F842L} to a similar extent as a mutation of Ser⁵² to Ala in Sui2 or expression of a Tif5^{W391F} allele with reduced affinity for Sui3 (Jennings and Pavitt, 2010) (Figure 3F). Moreover, this suppressive effect conferred by the Sui3^{S80A} allele, which was not

(C and D) Ser⁸⁰ in Sui3 critically defines its affinity for Tif5, but not for Gcd6. Cells expressing (from their genomes) WT Sui3 (WT), Sui3^{S80A} (S80A), or Sui3^{S80E} (S80E) together with Tif5-HA₆ (C) or Gcd6-HA₆ (D) were grown exponentially (EXP) or further treated for 30 min with 20 mM 3-AT. Lysates (input) and anti-HA immunoprecipitates (IPs [anti-HA]) were analyzed by immunoblotting using anti-HA and anti-Sui3 antibodies.

(E) Overexpression of Tif5 suppresses the 3-AT sensitivity of *sui3*^{S80A}, but not the one of *sui2*^{S52A} or *gcn2* Δ cells. WT and indicated mutant strains, overproducing or not overproducing Tif5 from a high-copy plasmid (*TIF5*^{hc}) were grown exponentially. They were then spotted (10-fold serial dilutions) and grown for 3 days at 30°C on SD + Arg/Trp or 100 mM 3-AT-containing plates as in Figure 2D. See also Figure S3.

(F) Mutation of Ser⁸⁰ to Ala in Sui3 suppresses the growth inhibition imposed by the expression of hyperactive Gcn2^{F842L}. WT and indicated mutant strains, expressing or not expressing plasmid-encoded hyperactive Gcn2^{F842L} were grown exponentially. They were then spotted (10-fold serial dilutions) and grown for 2 days at 30°C on SD-Ura/-Leu plates. In control experiments, the overexpression of plasmid-encoded Tif5 (*TIF5*^{hc}) abolished the *sui3*^{S80A}-mediated suppression of the slow-growth phenotype of Gcn2^{F842L}-expressing cells, while the overexpression of plasmid-encoded Tif5^{W391F} (*tif5*^{W391F}) suppressed the slow-growth phenotype of Gcn2^{F842L}-expressing cells.

(G) eIF2 α P analyses of exponentially growing strains used in (F). For details, see Figure 2E.

(H) Polysome profiles of exponentially growing WT and *sui3*^{S80A} mutant strains, expressing or not expressing plasmid-encoded hyperactive Gcn2^{F842L}. Unpaired Student's t tests were used to determine significant differences between WT cells expressing (red) or not expressing (gray) Gcn2^{F842L}, and between Gcn2^{F842L}-expressing WT (red) and *sui3*^{S80A} cells (blue). For details, see Figure 2F.

(I) Model for the role of Gcn2-mediated phosphorylation of eIF2 β /Sui3 in controlling translation initiation. In WT cells grown on amino acid-rich media (+AA; upper panel), eIF5/Tif5 binds eIF2 β /Sui3 primarily to fulfill its role as GAP of the eIF2-GTP-tRNA^{Met} TC during mRNA start site selection. eIF2B promotes eIF5 dissociation (Jennings et al., 2017) to facilitate eIF2B ϵ -mediated nucleotide exchange on eIF2 γ , thereby ensuring the recycling of eIF2-GDP to TC. In amino acid-starved WT cells (-AA; panel in the center), Gcn2 phosphorylates eIF2 α /Sui2 to tether eIF2B $\alpha\beta\delta$ and consequently prevent eIF2B ϵ -mediated nucleotide exchange on eIF2 γ . In parallel, Gcn2-mediated phosphorylation of eIF2 β ^{S80}/Sui3^{S80} recruits eIF5/Tif5 that acts as GDI to prevent spontaneous nucleotide exchange on eIF2 γ . eIF2 β ^{S80A}/Sui3^{S80A} (mutation marked with an asterisk in the lower panel) is compromised for eIF5/Tif5 recruitment in amino acid-starved cells. This allows some TC formation due to spontaneous nucleotide exchange on eIF2, despite proper eIF2 α P-mediated eIF2B $\alpha\beta\delta$ tethering. The basic model was adapted from Jennings and Pavitt (2010).

due to reduced eIF2 α P levels (Figure 3G), was fully abrogated by the overproduction of Tif5 (Figure 3F). Finally, the expression of Sui3^{S80A} also significantly suppressed the Gcn2^{F842L}-mediated reduction in global translation initiation (Figure 3H). Our results endorse and extend a model in which Gcn2-stimulated eIF2 β /Sui3-eIF5/Tif5 complex formation is part of the cellular response to amino acid starvation that contributes to the proper downregulation of translation initiation and consequently derepression of *GCN4* translation (Figure 3I).

Gcn2 engages in feedback inhibition through Gcn20-Thr⁹⁴/Ser⁹⁵ phosphorylation

Formation of the Gcn1-Gcn20 heterodimer is mediated by the N-terminal 118 amino acids of Gcn20 and the eukaryotic translation elongation factor 3 (eEF3)-like (EF3L) domain in Gcn1 (Vazquez de Aldana et al., 1995). Notably, mutation of the EF3L domain in Gcn1 reduces Gcn1-Gcn20 complex formation and confers a Gcn⁻ phenotype, which is consistent with the proposed role of the Gcn1-Gcn20 heterodimer in stimulating the activation of Gcn2 by uncharged tRNAs (Hinnebusch, 2005). Because Thr⁹⁴ and Ser⁹⁵ of Gcn20 are part of the interface that mediates Gcn1 binding, our data presented above raised the intriguing possibility that Gcn2 may engage in a feedback regulatory circuit by regulating Gcn1-Gcn20 complex formation through the phosphorylation of Gcn20. Our *in vitro* fluorescence spectroscopy studies with recombinant proteins supported this idea, as the affinity between the EF3L domain of Gcn1 (Gcn1^{EF3L}) and Gcn20 and the one between Gcn1^{EF3L} and Gcn20^{T94A,S95A} was ~33- and 18-fold higher, respectively, than the one between Gcn20^{T94E,S95E} and Gcn1^{EF3L} (Figure 4A). *In vivo*, both Gcn20 and Gcn20^{T94A,S95A} formed stable heterodimers with Gcn1 in exponentially growing cells as expected (Figure 4B). Treatment with 3-AT curtailed the association between Gcn20 and Gcn1, but not the one between Gcn20^{T94A,S95A} and Gcn1, suggesting that Gcn2-dependent phosphorylation of Thr⁹⁴/Ser⁹⁵ in Gcn20 antagonizes Gcn20-Gcn1 complex formation. In support of this notion, Gcn20^{T94E,S95E} was compromised for Gcn1 binding in exponentially growing cells and slightly more so in 3-AT-treated cells, which may be explained by the existence of additional Gcn2 target residues that have escaped detection by MS and that play a minor role in modulating the Gcn20-Gcn1 interaction (Figure 4B). Combined, these data therefore advocate a model in which Gcn2 engages in feedback inhibition through the phosphorylation of Gcn20-Thr⁹⁴/Ser⁹⁵, which favors disassembly of the Gcn1-Gcn20 complex.

Our analyses of the distal readouts for Gcn2 activity (i.e., *GCN4-LacZ* expression and polysome profiles) in *gcn20*^{T94A,S95A} and *gcn20*^{T94E,S95E} mutants also support this model (Figures 2C and 2F), even though the proximal Gcn2 readout, namely the eIF2 α P levels, appeared unchanged in these mutants (Figure 2E). We deemed it possible, however, that the sensitivity of our immunoblot analyses and/or the dynamic nature of the proposed regulatory loop may preclude proper resolution of the differences in eIF2 α P levels, which we expected to be rather moderate (i.e., within the range of 10%). To enhance the sensitivity of this assay, we therefore used the hyperactive *GCN2*^{F842L} allele that boosts eIF2 α P in exponentially growing cells (Figure 4C). Similar to the loss of Gcn20, expression of Gcn20^{T94E,S95E}, but

not expression of Gcn20^{T94A,S95A}, now clearly reduced the Gcn2^{F842L}-induced eIF2 α P levels (Figure 4C), which, as inferred from a control experiment using hemagglutinin (HA)-tagged variants of Gcn20 (Figure 4D), was not caused by Gcn20^{T94E,S95E} instability. In parallel, Gcn20^{T94E,S95E} also partially suppressed the slow-growth phenotype and the inhibition of global translation initiation that is mediated by the expression of the Gcn2^{F842L} allele (Figures 3H, 4E, and 4F). These data also perfectly match with the fact that the *gcn20-501* mutation was originally isolated as a suppressor of the slow-growth phenotype conferred by a hyperactive Gcn2 allele (Vazquez de Aldana et al., 1995). Thus, Gcn2 phosphorylates Gcn20 as part of an inhibitory feedback mechanism that contributes to the fine-tuning of the cellular response to amino acid starvation (Figure 4G).

Our study highlights that Gcn2 plays a substantially more intricate role in controlling translation initiation than has been previously appreciated. In this context, our phosphoproteome analyses further indicate that Gcn2 may, in parallel to Sui3 and Gcn20 studied here, also target (1) Yar1, which functions as a dedicated chaperone for the ribosomal protein Rps3 (Koch et al., 2012); (2) Yef3, the translation elongation factor 3 (Qin et al., 1987); (3) Sap185, which, in complex with the type 2A-related serine-threonine phosphatase Sit4, modulates TORC1-regulated, Gcn2-dependent translation (Rohde et al., 2004); and (4) Ssd1, an mRNA-binding protein that spatially and temporally controls the translation of specific mRNAs and/or regulates ribosome biogenesis (Jansen et al., 2009; Kurischko et al., 2011; Li et al., 2009) (Figure 1D). These observations warrant future studies that will address the intriguing possibility that the function of Gcn2 expands beyond its currently known role in translation initiation to a more universal role in shaping various aspects of translation in response to the availability of amino acids.

Limitations of study

The chosen bottom-up proteomics strategy ensures a maximum of phosphosite identifications given the technical setup. However, due to the proteolytic digestion of proteins before MS analysis, the crosstalk between different phosphosites cannot be studied and differential regulation of specific isoforms cannot be discriminated. As tandem MS (MS/MS) spectra do not always allow the unambiguous localization of specific phosphosites, which led to their exclusion from further analyses according to our data processing pipeline, some biologically meaningful hits may also have been lost in our MS analyses. Lastly, because our MS data did not cover the full repertoire of peptide variants (i.e. non-phosphorylated and singly or doubly phosphorylated peptide variants), we also could not determine the phosphosite occupancy (stoichiometry of phosphorylation) on Sui2, Sui3, and Gcn20.

A potential limitation with respect to the *in vitro* protein kinase assays that were carried out with the hyperactive Gcn2^{F842L} kinase may be that this allele could exhibit altered substrate recognition properties (although this is mitigated by the fact that this allele properly phosphorylates Sui2-Ser⁵² both *in vitro* and *in vivo*). In addition, it may be argued that our kinetic analyses of Gcn2 protein kinase activity toward eIF2 α and eIF2 β as independent substrates may not accurately reflect the *in vivo* conditions in which both proteins are part of the trimeric eIF2 complex.

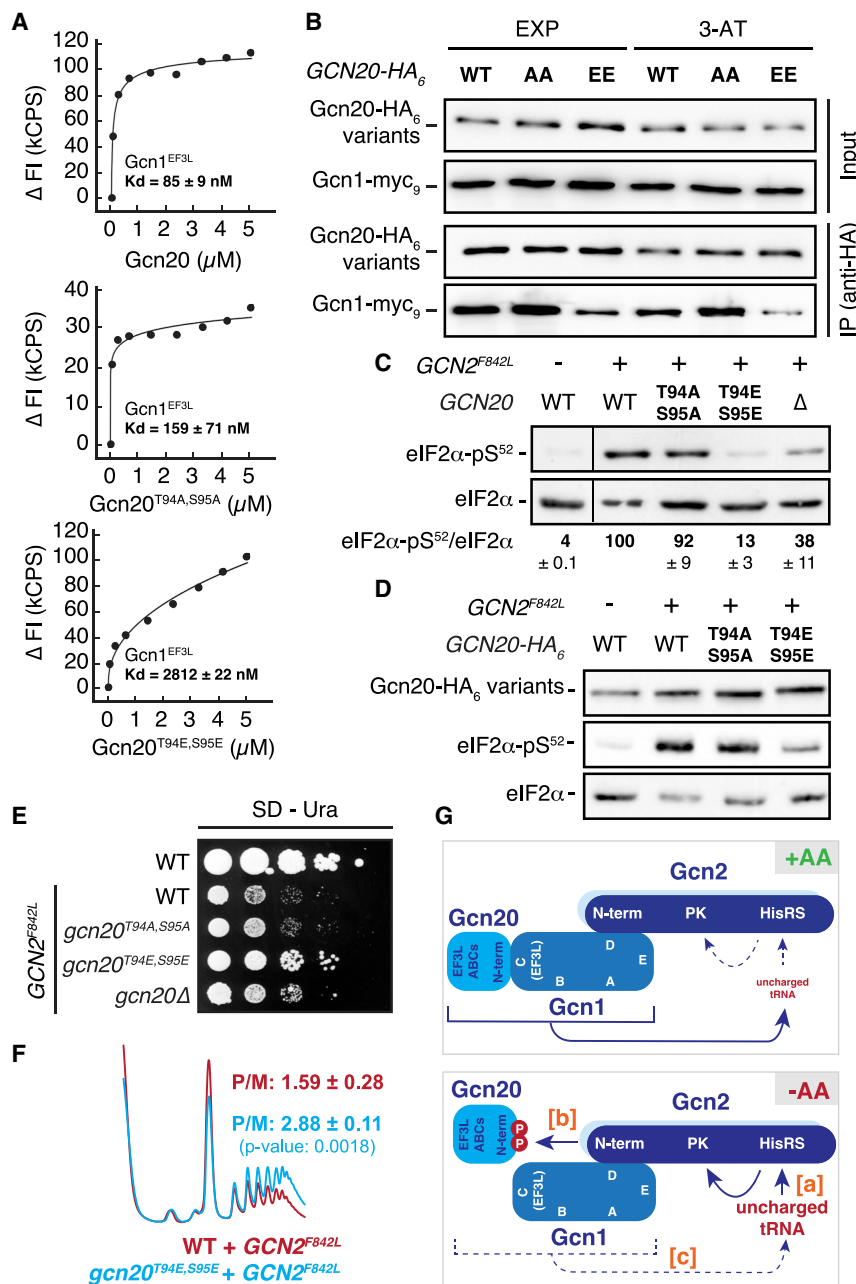


Figure 4. Gcn2 engages in feedback inhibition through Gcn2-Thr⁹⁴/Ser⁹⁵ phosphorylation

(A) Thr⁹⁴ and Ser⁹⁵ in Gcn2 critically define the affinity of Gcn2 for Gcn1 *in vitro*. The binding affinities of recombinant His₆-Gcn20, -Gcn20^{T94A,S95A}, and -Gcn20^{T94E,S95E} for the Alexa Fluor 488-labeled GST-EF3L domain of Gcn1 were determined by fluorescence dequenching. Three independent measurements were performed at room temperature, with SDs being <3% for each presented data point. The concentration of GST-EF3L was 50 nM. Dissociation constants (K_D ; $n = 3$; \pm SD) were calculated using nonlinear asymmetric sigmoidal regressions. Δ FI, relative difference in fluorescence intensity; kCPS, kilo counts per second.

(B) Thr⁹⁴ and Ser⁹⁵ in Gcn2 critically define the affinity of Gcn2 for Gcn1 *in vivo*. Cells expressing genomically WT Gcn20-HA₆ (WT), Gcn20^{T94A,S95A}-HA₆ (AA), or Gcn20^{T94E,S95E}-HA₆ (EE), together with Gcn1-myc₉, were grown exponentially (EXP) and then treated for 30 min with 20 mM 3-AT. Lysates (input) and anti-HA IPs (anti-HA) were analyzed by immunoblotting using anti-HA and anti-myc antibodies.

(C and D) Mutation of Thr⁹⁴ and Ser⁹⁵ to Glu in Gcn2 reduces the Gcn2^{F842L}-mediated hyperphosphorylation of eIF2 α . WT and indicated mutant strains, expressing (+) or not expressing (-) plasmid-encoded hyperactive Gcn2^{F842L}, were grown exponentially and analyzed for eIF2 α P levels using anti-eIF2 α -pSer⁵² and anti-eIF2 α antibodies as in Figure 2E (C and D). WT samples in (C) were run on the same gel as but not next to the other samples. Strains in (D) expressed HA₆-tagged Gcn20 variants that were visualized by using anti-HA antibodies. The mean ratios of eIF2 α -pS⁵²/eIF2 α ($n = 3$; \pm SD) in (C) were normalized to the one of Gcn2^{F842L}-expressing WT cells (set to 100%).

(E) Mutation of Thr⁹⁴ and Ser⁹⁵ to Glu in Gcn2 partially suppresses the growth inhibition imposed by the expression of hyperactive Gcn2^{F842L}. Exponentially growing strains (as in C) were spotted (10-fold serial dilutions) and grown for 3 days at 30°C on SD-Ura plates.

(F) Polysome profiles of exponentially growing WT and *gcn20*^{T94E,S95E} mutant strains expressing plasmid-encoded hyperactive Gcn2^{F842L}. For comparison, the data of the WT control expressing Gcn2^{F842L} (Figure 3H; red) are shown again. The unpaired Student's *t* test was used to determine the significant difference between Gcn2^{F842L}-expressing WT (red) and *gcn20*^{T94E,S95E} cells (blue). For details, see Figure 2F.

(G) Gcn2-mediated phosphorylation of Gcn2 is part of an inhibitory feedback mechanism. The Gcn1-Gcn2 heterodimer stimulates the activation of Gcn2 by uncharged tRNAs as proposed earlier; the respective model including the domain nomenclature and representation of Gcn2 as a dimer was adapted from Hinnebusch (2005). In amino acid-replete conditions (+AA), the levels of uncharged tRNAs, and hence Gcn2 activity, are low. This favors hypophosphorylation of Gcn2 and Gcn1-Gcn2 heterodimer formation, which primes Gcn2 to optimally sense uncharged tRNAs. Upon amino acid starvation (-AA), accumulating uncharged tRNAs activate Gcn2 (a), which phosphorylates Thr⁹⁴/Ser⁹⁵ in Gcn2 (red circled "P") to release it from Gcn1 (b), and thereby reduce the Gcn1-Gcn2-mediated stimulation of Gcn2 by uncharged tRNAs (c). Notably, the proposed feedback mechanism possibly also operates at a very low level when cells are growing in the presence of amino acids. The dashed lines indicate reduced function. EF3L, eukaryotic elongation factor 3-like domain; EF3L ABCs, EF3-related ATP-binding cassettes; HisRS, histidyl-tRNA synthase-related tRNA-binding domain; PK, protein kinase domain; A-E, subdomains of Gcn1.

Gcn2 kinase assays with entire eIF2 complexes that carry or do not carry Sui2^{S52A} and/or Sui3^{S80A} mutations, may therefore more closely mimic the *in vivo* situation. A caveat of such assays,

however, is that the Gcn2-target residues in Sui2 and Sui3 likely compete with each other for being phosphorylated by Gcn2 and that the respective phosphorylation events cannot be quantified

individually on WT eIF2 because both proteins exactly comigrate on SDS gels.

Finally, our genetic, biochemical, and physiological experiments indicate that cells expressing Sui3^{S80A} and Gcn20^{T94E/S95E} maintain higher TC levels under conditions in which Gcn2 efficiently phosphorylates eIF2 α (e.g., nutrient starvation, rapamycin treatment). These differences in TC levels, however, are likely close to the detection limit beyond which polysome profile analyses can discriminate global translation initiation defects with statistical significance. Because the much more sensitive *GCN4-LacZ* assay was able to delineate the effects of the Sui3^{S80A} and Gcn20^{T94E/S95E} alleles, it will be interesting to characterize the translomate (using polysome and/or ribosome profiling) of respective mutants to explore the possibility that Sui3^{S80A} and Gcn20^{T94E/S95E} may, rather than globally controlling translation initiation, specifically affect the expression of a subset of growth-related mRNAs.

STAR★METHODS

Detailed methods are provided in the online version of this paper and include the following:

- KEY RESOURCES TABLE
- RESOURCE AVAILABILITY
 - Lead contact
 - Materials availability
 - Data and code availability
- EXPERIMENTAL MODEL AND SUBJECT DETAILS
- METHOD DETAILS
 - Yeast strains, plasmids, and growth conditions
 - MS sample preparation, phosphopeptide enrichment, and LC-MS/MS analyses
 - Protein purification
 - *In vitro* Gcn2 kinase assay
 - Co-immunoprecipitation and immunoblot analyses
 - β -Galactosidase assays
 - Polysome profile analysis
 - Fluorescence spectroscopy
- QUANTIFICATION AND STATISTICAL ANALYSIS

SUPPLEMENTAL INFORMATION

Supplemental information can be found online at <https://doi.org/10.1016/j.molcel.2021.02.037>.

ACKNOWLEDGMENTS

We thank Susanne Stumpe and Malika Jaquenoud for technical assistance; Alan Hinnebusch, Graham Pavitt, and Leoš Valásek for strains and/or plasmids; Wolfgang Seufert for antibodies; Marie-Pierre Péli-Gulli for critically reading the manuscript; and Eva Sýkorová and the Institute of Biophysics of the Czech Academy of Sciences for providing their facilities during the COVID-19 restrictions in Switzerland. This research was supported by the Canton of Fribourg and the Swiss National Science Foundation, Switzerland (to D.K., J.D., and C.D.V.).

AUTHOR CONTRIBUTIONS

Conceptualization, L.D. and C.D.V.; methodology, L.D., M.S., Z.H., D.K., J.D., and C.D.V.; investigation, L.D., M.S., Z.H., B.P., and G.M.G.O.; writing – orig-

inal draft, J.D. and C.D.V.; writing – review & editing, L.D., D.K., J.D., and C.D.V.; funding acquisition, resources, & supervision, D.K., J.D., and C.D.V.

DECLARATION OF INTERESTS

The authors declare no competing interests.

Received: September 21, 2020

Revised: December 9, 2020

Accepted: February 24, 2021

Published: March 19, 2021

REFERENCES

- Albert, V., and Hall, M.N. (2015). mTOR signaling in cellular and organismal energetics. *Curr. Opin. Cell Biol.* 33, 55–66.
- Antony, A.C., and Alone, P.V. (2017). Defect in the GTPase activating protein (GAP) function of eIF5 causes repression of *GCN4* translation. *Biochem. Biophys. Res. Commun.* 486, 1110–1115.
- Asano, K., Krishnamoorthy, T., Phan, L., Pavitt, G.D., and Hinnebusch, A.G. (1999). Conserved bipartite motifs in yeast eIF5 and eIF2B ϵ , GTPase-activating and GDP-GTP exchange factors in translation initiation, mediate binding to their common substrate eIF2. *EMBO J.* 18, 1673–1688.
- Binda, M., Péli-Gulli, M.P., Bonfils, G., Panchaud, N., Urban, J., Sturgill, T.W., Loewith, R., and De Virgilio, C. (2009). The Vam6 GEF controls TORC1 by activating the EGO complex. *Mol. Cell* 35, 563–573.
- Boersema, P.J., Raijmakers, R., Lemeer, S., Mohammed, S., and Heck, A.J. (2009). Multiplex peptide stable isotope dimethyl labeling for quantitative proteomics. *Nat. Protoc.* 4, 484–494.
- Brachmann, C.B., Davies, A., Cost, G.J., Caputo, E., Li, J., Hieter, P., and Boeke, J.D. (1998). Designer deletion strains derived from *Saccharomyces cerevisiae* S288C: a useful set of strains and plasmids for PCR-mediated gene disruption and other applications. *Yeast* 14, 115–132.
- Cherkasova, V.A., and Hinnebusch, A.G. (2003). Translational control by TOR and TAP42 through dephosphorylation of eIF2 α kinase GCN2. *Genes Dev.* 17, 859–872.
- Cox, J., and Mann, M. (2008). MaxQuant enables high peptide identification rates, individualized p.p.b.-range mass accuracies and proteome-wide protein quantification. *Nat. Biotechnol.* 26, 1367–1372.
- Demetriades, C., Doumpas, N., and Teleman, A.A. (2014). Regulation of TORC1 in response to amino acid starvation via lysosomal recruitment of TSC2. *Cell* 156, 786–799.
- Dever, T.E., Feng, L., Wek, R.C., Cigan, A.M., Donahue, T.F., and Hinnebusch, A.G. (1992). Phosphorylation of initiation factor 2 α by protein kinase GCN2 mediates gene-specific translational control of GCN4 in yeast. *Cell* 68, 585–596.
- Donahue, T.F., and Cigan, A.M. (1988). Genetic selection for mutations that reduce or abolish ribosomal recognition of the *HIS4* translational initiator region. *Mol. Cell. Biol.* 8, 2955–2963.
- Dong, J., Qiu, H., Garcia-Barrio, M., Anderson, J., and Hinnebusch, A.G. (2000). Uncharged tRNA activates GCN2 by displacing the protein kinase moiety from a bipartite tRNA-binding domain. *Mol. Cell* 6, 269–279.
- Generoso, W.C., Gottardi, M., Oreb, M., and Boles, E. (2016). Simplified CRISPR-Cas genome editing for *Saccharomyces cerevisiae*. *J. Microbiol. Methods* 127, 203–205.
- Guarente, L. (1983). Yeast promoters and *lacZ* fusions designed to study expression of cloned genes in yeast. *Methods Enzymol.* 101, 181–191.
- Hatakeyama, R., and De Virgilio, C. (2019). TORC1 specifically inhibits microautophagy through ESCRT-0. *Curr. Genet.* 65, 1243–1249.
- Hinnebusch, A.G. (1985). A hierarchy of trans-acting factors modulates translation of an activator of amino acid biosynthetic genes in *Saccharomyces cerevisiae*. *Mol. Cell. Biol.* 5, 2349–2360.
- Hinnebusch, A.G. (1996). Translational control of *GCN4*: Gene-specific regulation by phosphorylation of eIF2. In *Translational Control*, J.W.B. Hershey, M.B.

- Mathews, and N. Sonenberg, eds. (Cold Spring Harbor Laboratory Press), pp. 199–244.
- Hinnebusch, A.G. (2005). Translational regulation of *GCN4* and the general amino acid control of yeast. *Annu. Rev. Microbiol.* **59**, 407–450.
- Hu, Z., Raucchi, S., Jaquenoud, M., Hatakeyama, R., Stumpe, M., Rohr, R., Reggiori, F., De Virgilio, C., and Dengjel, J. (2019). Multilayered control of protein turnover by TORC1 and Atg1. *Cell Rep.* **28**, 3486–3496.e6.
- Janke, C., Magiera, M.M., Rathfelder, N., Taxis, C., Reber, S., Maekawa, H., Moreno-Borchart, A., Doenges, G., Schwob, E., Schiebel, E., and Knop, M. (2004). A versatile toolbox for PCR-based tagging of yeast genes: new fluorescent proteins, more markers and promoter substitution cassettes. *Yeast* **21**, 947–962.
- Janovič, T., Stojaspal, M., Veverka, P., Horáková, D., and Hofr, C. (2019). Human Telomere Repeat Binding Factor TRF1 Replaces TRF2 Bound to Shelterin Core Hub TIN2 when TPP1 Is Absent. *J. Mol. Biol.* **431**, 3289–3301.
- Jansen, J.M., Wanless, A.G., Seidel, C.W., and Weiss, E.L. (2009). Cbk1 regulation of the RNA-binding protein Ssd1 integrates cell fate with translational control. *Curr. Biol.* **19**, 2114–2120.
- Jennings, M.D., and Pavitt, G.D. (2010). eIF5 has GDI activity necessary for translational control by eIF2 phosphorylation. *Nature* **465**, 378–381.
- Jennings, M.D., Kershaw, C.J., White, C., Hoyle, D., Richardson, J.P., Costello, J.L., Donaldson, I.J., Zhou, Y., and Pavitt, G.D. (2016). eIF2β is critical for eIF5-mediated GDP-dissociation inhibitor activity and translational control. *Nucleic Acids Res.* **44**, 9698–9709.
- Jennings, M.D., Kershaw, C.J., Adomavicius, T., and Pavitt, G.D. (2017). Fail-safe control of translation initiation by dissociation of eIF2α phosphorylated ternary complexes. *eLife* **6**, e24542.
- Jia, M.H., Larossa, R.A., Lee, J.M., Rafalski, A., Derose, E., Gonye, G., and Xue, Z. (2000). Global expression profiling of yeast treated with an inhibitor of amino acid biosynthesis, sulfometuron methyl. *Physiol. Genomics* **3**, 83–92.
- Kilberg, M.S., Shan, J., and Su, N. (2009). ATF4-dependent transcription mediates signaling of amino acid limitation. *Trends Endocrinol. Metab.* **20**, 436–443.
- Kim, E., Goraksha-Hicks, P., Li, L., Neufeld, T.P., and Guan, K.L. (2008). Regulation of TORC1 by Rag GTPases in nutrient response. *Nat. Cell Biol.* **10**, 935–945.
- Koch, B., Mitterer, V., Niederhauser, J., Stanborough, T., Murat, G., Rechberger, G., Bergler, H., Kressler, D., and Pertschy, B. (2012). Yar1 protects the ribosomal protein Rps3 from aggregation. *J. Biol. Chem.* **287**, 21806–21815.
- Krishnamoorthy, T., Pavitt, G.D., Zhang, F., Dever, T.E., and Hinnebusch, A.G. (2001). Tight binding of the phosphorylated alpha subunit of initiation factor 2 (eIF2α) to the regulatory subunits of guanine nucleotide exchange factor eIF2B is required for inhibition of translation initiation. *Mol. Cell Biol.* **21**, 5018–5030.
- Kurischko, C., Kim, H.K., Kuravi, V.K., Pratzka, J., and Luca, F.C. (2011). The yeast Cbk1 kinase regulates mRNA localization via the mRNA-binding protein Ssd1. *J. Cell Biol.* **192**, 583–598.
- Laplante, M., and Sabatini, D.M. (2012). mTOR signaling in growth control and disease. *Cell* **149**, 274–293.
- Li, L., Lu, Y., Qin, L.X., Bar-Joseph, Z., Werner-Washburne, M., and Breeden, L.L. (2009). Budding yeast *SSD1-V* regulates transcript levels of many longevity genes and extends chronological life span in purified quiescent cells. *Mol. Biol. Cell* **20**, 3851–3864.
- Mohammad-Qureshi, S.S., Haddad, R., Hemingway, E.J., Richardson, J.P., and Pavitt, G.D. (2007). Critical contacts between the eukaryotic initiation factor 2B (eIF2B) catalytic domain and both eIF2β and -2γ mediate guanine nucleotide exchange. *Mol. Cell Biol.* **27**, 5225–5234.
- Mueller, P.P., and Hinnebusch, A.G. (1986). Multiple upstream AUG codons mediate translational control of *GCN4*. *Cell* **45**, 201–207.
- Natarajan, K., Meyer, M.R., Jackson, B.M., Slade, D., Roberts, C., Hinnebusch, A.G., and Marton, M.J. (2001). Transcriptional profiling shows that Gcn4p is a master regulator of gene expression during amino acid starvation in yeast. *Mol. Cell Biol.* **21**, 4347–4368.
- Olsen, J.V., Blagoev, B., Gnäd, F., Macek, B., Kumar, C., Mortensen, P., and Mann, M. (2006). Global, in vivo, and site-specific phosphorylation dynamics in signaling networks. *Cell* **127**, 635–648.
- Pedruzzi, I., Dubouloz, F., Cameroni, E., Wanke, V., Roosen, J., Winderickx, J., and De Virgilio, C. (2003). TOR and PKA signaling pathways converge on the protein kinase Rim15 to control entry into G₀. *Mol. Cell* **12**, 1607–1613.
- Perez-Riverol, Y., Csordas, A., Bai, J., Bernal-Llinares, M., Hewapathirana, S., Kundu, D.J., Inuganti, A., Griss, J., Mayer, G., Eisenacher, M., et al. (2019). The PRIDE database and related tools and resources in 2019: improving support for quantification data. *Nucleic Acids Res.* **47** (D1), D442–D450.
- Perzmaier, A.F., Richter, F., and Seufert, W. (2013). Translation initiation requires cell division cycle 123 (Cdc123) to facilitate biogenesis of the eukaryotic initiation factor 2 (eIF2). *J. Biol. Chem.* **288**, 21537–21546.
- Qin, S.L., Moldave, K., and McLaughlin, C.S. (1987). Isolation of the yeast gene encoding elongation factor 3 for protein synthesis. *J. Biol. Chem.* **262**, 7802–7807.
- Qiu, H., Hu, C., Dong, J., and Hinnebusch, A.G. (2002). Mutations that bypass tRNA binding activate the intrinsically defective kinase domain in GCN2. *Genes Dev.* **16**, 1271–1280.
- Rohde, J.R., Campbell, S., Zurita-Martinez, S.A., Cutler, N.S., Ashe, M., and Cardenas, M.E. (2004). TOR controls transcriptional and translational programs via Sap-Sit4 protein phosphatase signaling effectors. *Mol. Cell Biol.* **24**, 8332–8341.
- Sancak, Y., Peterson, T.R., Shaul, Y.D., Lindquist, R.A., Thoreen, C.C., Bar-Peled, L., and Sabatini, D.M. (2008). The Rag GTPases bind raptor and mediate amino acid signaling to mTORC1. *Science* **320**, 1496–1501.
- Szklarczyk, D., Gable, A.L., Lyon, D., Junge, A., Wyder, S., Huerta-Cepas, J., Simonovic, M., Doncheva, N.T., Morris, J.H., Bork, P., et al. (2019). STRING v11: protein-protein association networks with increased coverage, supporting functional discovery in genome-wide experimental datasets. *Nucleic Acids Res.* **47** (D1), D607–D613.
- Thakur, A., Marler, L., and Hinnebusch, A.G. (2019). A network of eIF2β interactions with eIF1 and Met-tRNA, promotes accurate start codon selection by the translation preinitiation complex. *Nucleic Acids Res.* **47**, 2574–2593.
- Tyanova, S., Temu, T., Sinitcyn, P., Carlson, A., Hein, M.Y., Geiger, T., Mann, M., and Cox, J. (2016). The Perseus computational platform for comprehensive analysis of (prote)omics data. *Nat. Methods* **13**, 731–740.
- Vattem, K.M., and Wek, R.C. (2004). Reinitiation involving upstream ORFs regulates *ATF4* mRNA translation in mammalian cells. *Proc. Natl. Acad. Sci. USA* **101**, 11269–11274.
- Vazquez de Aldana, C.R.V., Marton, M.J., and Hinnebusch, A.G. (1995). GCN20, a novel ATP binding cassette protein, and GCN1 reside in a complex that mediates activation of the eIF-2α kinase GCN2 in amino acid-starved cells. *EMBO J.* **14**, 3184–3199.
- Wolfson, R.L., and Sabatini, D.M. (2017). The dawn of the age of amino acid sensors for the mTORC1 pathway. *Cell Metab.* **26**, 301–309.
- Ye, J., Palm, W., Peng, M., King, B., Lindsten, T., Li, M.O., Koumenis, C., and Thompson, C.B. (2015). GCN2 sustains mTORC1 suppression upon amino acid deprivation by inducing Sestrin2. *Genes Dev.* **29**, 2331–2336.
- Yuan, W., Guo, S., Gao, J., Zhong, M., Yan, G., Wu, W., Chao, Y., and Jiang, Y. (2017). General control nonderepressible 2 (GCN2) kinase inhibits target of rapamycin complex 1 in response to amino acid starvation in *Saccharomyces cerevisiae*. *J. Biol. Chem.* **292**, 2660–2669.
- Zhu, S., Sobolev, A.Y., and Wek, R.C. (1996). Histidyl-tRNA synthetase-related sequences in GCN2 protein kinase regulate *in vitro* phosphorylation of eIF-2. *J. Biol. Chem.* **271**, 24989–24994.

STAR★METHODS

KEY RESOURCES TABLE

REAGENT or RESOURCE	SOURCE	IDENTIFIER
Antibodies		
Rabbit phospho-EIF2S1 (Ser 52) (1:2'000)	Invitrogen	44-728G
Rabbit anti-Sui2 (1:2'000)	Perzmaier et al., 2013	N/A
Rabbit anti-Sui3 (1:2'000)	Perzmaier et al., 2013	N/A
Mouse anti-c-Myc (9E10) (1:3'000)	Santa Cruz Biotechnology	sc-40
Mouse anti-HA (12CA5) (1:1'000)	De Virgilio lab	N/A
Rabbit anti-Sch9-pThr ⁷³⁷ (1:10'000)	De Virgilio lab	N/A
Goat anti-Sch9 (1:1'000)	De Virgilio lab	N/A
Goat anti-mouse IgG-HRP conjugate (1:3'000)	BIO-RAD	1706516
Goat anti-rabbit IgG-HRP conjugate (1:3'000)	BIO-RAD	1706515
Rabbit anti-goat IgG-HRP conjugate (1:5'000)	BIO-RAD	1721034
Peroxidase AffiniPure Goat Anti-Mouse IgG, light chain specific (1:3'000)	Jackson ImmunoResearch	115-035-174
Bacterial strains		
<i>E. coli</i> Rosetta (DE3)	Novagen	70954
<i>E. coli</i> DH5 α	CGSC	12384
Chemicals, peptides, and recombinant proteins		
[γ - ³² P]ATP	Hartmann Analytic	SCP301
2-nitrophenyl- β -D-galactopyranoside	Sigma-Aldrich	73660
3-amino-1-1,2,4-triazole	Acros Organics	264571000
Adenosine-5'-triphosphate disodium salt hydrate	Sigma-Aldrich	A2383
Alexa Fluor 488 5-TFP	Life Technologies	A30005
Ammonium sulfate	MP Biomedicals	4808211
Anti-FLAG M2 magnetic beads	Sigma-Aldrich	M8823
Arg10	Sigma-Aldrich	608033
Arg6	Sigma-Aldrich	643440
C18 Cartridges	Macherey-Nagel	731802
Complete EDTA-free Protease Inhibitor Cocktail	Roche	11-697-498-001
Cycloheximide	Sigma-Aldrich	C7698-5G
Drop-out Mix Synthetic, minus Ade, Arg, His, Leu, Lys, Trp, Ura	US Biological	D9545
DTT	Applichem	A1101-0025
GCN2, active	Millipore	14-934
Glutathione MagBeads	GenScript	L00327
HR-X Column	Macherey-Nagel	730936P45
Lys4	Sigma-Aldrich	616192
Lys8	Sigma-Aldrich	608041
Lys-C	FUJIFILM Wako Pure Chemical Corporation	129-02541
MS-grade Acetonitrile	VWR	20060-320
NaF	Sigma-Aldrich	215309
Ni-charged MagBeads	GenScript	L00295
Nonidet P-40	Applichem	A1694-0250
Pefabloc	Sigma-Aldrich	76307
PhosSTOP	Roche	04-906-837-001

(Continued on next page)

Continued

REAGENT or RESOURCE	SOURCE	IDENTIFIER
Pierce Anti-HA Magnetic Beads	Thermo Scientific	88837
PMSF	Calbiochem	52332
Rapamycin	LC Laboratories	R-5000
ReproSil-Pur 120 C18-AQ, 1.9 μm	Dr. Maisch	r119.aq.
Side-A-Lyzer 10K MWCO MINI dialysis device	Thermo Scientific	88404
Sui3(68-89) peptide	GenScript	PTDDIAEALGELSLKKKKKKTK
Sui3(68-89; pSer ⁸⁰) peptide	GenScript	PTDDIAEALGEL[pSer]LKKKKKKTK
SYPRO Ruby Protein Gel Stain	Sigma-Aldrich	S4942
TCA	Sigma-Aldrich	27242
TFA	Sigma-Aldrich	302031
Titanium dioxide	GL Sciences	5020-75010
Trypsin	Promega	V5113
Yeast nitrogen base	CONDA	1553-00
YPD broth	US Biological	Y2075
β-Glycerophosphate disodium salt hydrate	Sigma-Aldrich	G9422

Critical commercial assays

ECL Western Blotting Detection	GE Healthcare	RPN2106
Radiance Plus Sensitive ECL	Azure Biosystems	AC2103
QuikChange Multi Site-Directed Mutagenesis Kit	Agilent	200514

Deposited data

MS-RAW files	ProteomeXchange	PXD021109
Original Data	Mendeley Data	https://doi.org/10.17632/g6557yvmf5.1

Experimental models: organisms/strains

YL515	Binda et al., 2009	[BY4741/2] <i>MATα</i> ; <i>his3Δ1 leu2Δ0 ura3Δ0</i>
YL516 (Figures 2C–2F , 3E–3H , 4C , 4E , 4F , S3 , and S4)	Binda et al., 2009	[BY4741/2] <i>MATα</i> ; <i>his3Δ1 leu2Δ0 ura3Δ0</i>
MJ5682 (Figure 1 ; Table S1)	Hu et al., 2019	[YL515] <i>arg4Δ::hisMX4 lys2Δ::hphNT1</i>
LD5759 (Figure 1 ; Table S1)	This study	[MJ5682] <i>gcn2Δ::natNT2</i>
LD5797 (Figure 1 ; Table S1)	This study	[MJ5682] <i>sui2^{S52A}</i>
HQY346 (Figures 2A , 2B , and S2B)	Qiu et al., 2002	<i>MATα</i> ; <i>ura3-52 leu2-3 leu2-112 trp1-Δ63 gcn2Δ gcd2Δ::hisG (GCD2^{K627T}, TRP1) GAL2⁺</i>
GMGO005 (Figures 2C–2F , 3E , S3 , and S4)	This study	[YL515] <i>gcn2Δ::hphNT1</i>
LD5945 (Figures 2C–2F , 3E–3G , S3 , and S4)	This study	[YL516] <i>sui2^{S52A}</i>
LD5946 (Figures 2C–2F , 3E–3H , S3 , and S4)	This study	[YL516] <i>sui3^{S80A}</i>
LD6055 (Figures 2C–2F , 3E–3G , S3 , and S4)	This study	[YL516] <i>sui3^{S80A} sui2^{S52A}</i>
LD6201 (Figures 2C–2F , 3E–3G , S3 , and S4)	This study	[YL515] <i>sui3^{S80E}</i>
LD6130 (Figures 2C–2F , 4C , 4E , and S3)	This study	[YL516] <i>gcn20^{T94A,S95A}</i>
LD6219 (Figures 2C–2F , 4C , 4E , 4F , and S3)	This study	[YL516] <i>gcn20^{T94E,S95E}</i>
LD6287 (Figures 2C–2E , 4C , 4E , and S3)	This study	[YL516] <i>gcn20Δ::hphNT1</i>
LD6400 (Figures 2C and 2D and S3)	This study	[LD6201] <i>gcn2Δ::hphNT1</i>
LD6035 (Figure 3D)	This study	[YL516] <i>GCD6-HA₆::natNT2</i>
LD6047 (Figure 3D)	This study	[LD6035] <i>sui3^{S80A}</i>
LD6274 (Figure 3D)	This study	[LD6201] <i>GCD6-HA₆::natNT2</i>
LD6036 (Figure 3C)	This study	[YL515] <i>TIF5-HA₆::natNT2</i>
LD6067 (Figure 3C)	This study	[LD6036] <i>sui3^{S80A}</i>
LD6273 (Figure 3C)	This study	[LD6201] <i>TIF5-HA₆::natNT2</i>
LD6279 (Figures 4B and 4D)	This study	[YL515] <i>GCN1-myc₉::hphNT1</i> <i>GCN20-HA₆::natNT2</i>

(Continued on next page)

Continued

REAGENT or RESOURCE	SOURCE	IDENTIFIER
LD6280 (Figures 4B and 4D)	This study	[YL516] <i>GCN1-myc_g::hphNT1 gcn20^{T94A,S95A}-HA₆::natNT2</i>
LD6281 (Figures 4B and 4D)	This study	[YL516] <i>GCN1-myc_g::hphNT1 gcn20^{T94E,S95E}-HA₆::natNT2</i>
KT1960 (Figure S1; Table S2)	Pedruzzi et al., 2003	<i>MATα; ura3-52 leu2 his3 trp1</i>
MP5050 (Figure S1; Table S2)	This study	[KT1960] <i>gcn2Δ::hphNT1</i>
GMGO021 (Figure S1)	This study	[KT1960] <i>gcn4Δ::kanMX4</i>
GMGO022 (Figure S1)	This study	[KT1960] <i>gcn2Δ::hphNT1 gcn4Δ::kanMX4</i>
Recombinant DNA		
p3808 (Figures 2A, 2B, and S2)	This study	[pET-15b] <i>SUI3</i>
p3809 (Figures 2A, 2B, 4A, and S2)	This study	[pET-15b] <i>GCN20</i>
p3807 (Figure S2)	This study	[pET-15b] <i>SUI2</i>
pLD4013 (Figure 2A)	This study	[pET-15b] <i>sui3^{S80A}</i>
pLD4015 (Figures 2A and 4A)	This study	[pET-15b] <i>gcn20^{T94A,S95A}</i>
pLD4014 (Figure 4A)	This study	[pET-15b] <i>gcn20^{T94E,S95E}</i>
pLD4019 (Figure 3B)	This study	[pGEX-3X] <i>GCD6</i>
pLD4020 (Figure 3A)	This study	[pGEX-3X] <i>TIF5</i>
pLD4016 (Figure 4A)	This study	[pGEX-3X] <i>EF3L(GCN1¹³³¹⁻¹⁶⁷⁰)</i>
pDH103 (Figures 2A and 2B)	Dong et al., 2000	2 μ , <i>URA3, GAL1p-GCN2-FLAG-His₆</i>
pLD4074 (Figures 2A, 2B, and S2)	This study	2 μ , <i>URA3, GAL1p-GCN2^{F842L}-FLAG-His₆</i>
pDH109 (Figures 2A and 2B)	Dong et al., 2000	2 μ , <i>URA3, GAL1p-gcn2^{K628R}-FLAG-His₆</i>
p180 (Figure 2C)	Hinnebusch, 1985	CEN/ARS, <i>URA3, GCN4-LacZ</i>
p367 (Figure S4)	Donahue and Cigan, 1988	CEN/ARS, <i>URA3, HIS4-AUG-LacZ</i>
p391 (Figure S4)	Donahue and Cigan, 1988	CEN/ARS, <i>URA3, his4-UUG-LacZ</i>
pLD4079 (Figure S4)	This study	CEN/ARS, <i>LEU2, tif5^{G31R}</i>
YE _p TIF5-FL (Figures 3E–3G and S3)	Asano et al., 1999	2 μ , <i>LEU2, TIF5-FLAG</i>
pHQ1103 (Figures 3F–3H and 4C–4F)	Qiu et al., 2002	CEN/ARS, <i>URA3, GCN2^{F842L}</i>
pAV1936 (Figures 3F and 3G)	Jennings and Pavitt, 2010	2 μ , <i>LEU2, tif5^{W391F}-FLAG</i>
pRS413 (Figures 2C–2E, 3C–3E, 4B, S1, and S3; Table S2)	Brachmann et al., 1998	CEN/ARS, <i>HIS3</i>
pRS415 (Figures 2D, 3E–3G, S3, and S4)	Brachmann et al., 1998	CEN/ARS, <i>LEU2</i>
pRS416 (Figures 2D, 3E–3H, 4C–4E, S1, and S3; Table S2)	Brachmann et al., 1998	CEN/ARS, <i>URA3</i>
Software and algorithms		
ImageJ	NIH	https://imagej.nih.gov/ij/index.html
MaxQuant	Cox and Mann, 2008	https://maxquant.net/maxquant/
Perseus	Tyanova et al., 2016	https://maxquant.net/perseus/
Prism 8	Graphpad	https://www.graphpad.com/scientific-software/prism/
Motif Analysis	NIH	https://www.phosphosite.org/staticMotifAnalysis.action

RESOURCE AVAILABILITY**Lead contact**

Further information and requests for resources and reagents should be directed to and will be fulfilled by the Lead Contact, Claudio De Virgilio (Claudio.DeVirgilio@unifr.ch).

Materials availability

All unique/stable reagents generated in this study are available from the Lead Contact.

Data and code availability

The mass spectrometry proteomics data have been deposited to the ProteomeXchange Consortium via the PRIDE partner repository with the dataset identifier PRIDE Archive: PXD021109 (Perez-Riverol et al., 2019). Source data for gel images and graphs can be found in Mendeley Data:

<https://doi.org/10.17632/g6557yvmf5.1>

EXPERIMENTAL MODEL AND SUBJECT DETAILS

Saccharomyces cerevisiae strains used in this study are listed in the [Key resources table](#). They were grown as described in [Method details](#) below. Recombinant proteins were expressed in *Escherichia coli* Rosetta (DE3) and cloning procedures were carried out in *E. coli* DH5 α .

METHOD DETAILS

Yeast strains, plasmids, and growth conditions

Saccharomyces cerevisiae strains and plasmids are listed in [Key resources table](#). CRISPR-Cas9 genome editing was performed as described (Generoso et al., 2016). Gene deletion and gene tagging were performed using the pFA6a system-based PCR-toolbox (Janke et al., 2004). Plasmids used for recombinant Sui2, Sui3, and Gcn20 production were codon-optimized for expression in *E. coli* and purchased from GenScript. Plasmid mutagenesis was performed using the QuikChange Multi Site-Directed Mutagenesis Kit (Agilent). Unless otherwise stated, yeast strains were grown to mid-log phase in SD medium (0.17% yeast nitrogen base, 0.5% ammonium sulfate and 2% glucose). For *in vivo* SILAC experiments, yeast strains were grown in synthetic dextrose complete medium (or in SD medium lacking histidine and uracil in case of leucine starvation experiments) containing either non-labeled or labeled lysine and arginine variants: “Heavy” L-arginine-¹³C₆-¹⁵N₄ (Arg10) and L-lysine-¹³C₆-¹⁵N₂ (Lys8), or “medium” L-arginine-¹³C₆ (Arg6) and L-lysine-²H₄ (Lys4) amino acids (Sigma-Aldrich) were used as labels. Cells were treated or not with 200 ng mL⁻¹ rapamycin for 30 min, or starved for leucine for 1 h. Note that for leucine starvation experiments, the cells were auxotrophic for leucine.

MS sample preparation, phosphopeptide enrichment, and LC-MS/MS analyses

MS samples and LC-MS/MS analyses were performed as described in Hu et al. (2019). Briefly, yeast strains were grown in synthetic dextrose complete medium containing either non-labeled or labeled lysine and arginine variants (see “[Yeast strains, plasmids, and growth conditions](#)”). Dried TCA-treated cell pellets (100 mg) of each labeling were mixed, proteins extracted in 8 M urea, and digested by Lys-C (Lysyl Endopeptidase, WAKO) for 4 h at room temperature. The concentration of urea was diluted to 1 M before overnight trypsin digestion (Promega). The second day, peptides were purified by SPE using HR-X columns in combination with C18 cartridges (Macherey-Nagel), eluates were frozen in liquid nitrogen and lyophilized overnight. For one biological replicate of leucine starvation, dimethyl labeling was used instead of SILAC labeling and differentially labeled peptides were mixed (Boersema et al., 2009). The third day, peptides were fractionated by HpH reversed phase chromatography, fractions were acidified, frozen in liquid nitrogen, and lyophilized overnight. The fourth day, the dry peptides were suspended in 200 μ l 80% acetonitrile with 1% TFA for phosphopeptide enrichment. For both *in vitro* and *in vivo* experiments, phosphopeptides were enriched by TiO₂ beads (GL Sciences). The tip flow-through was stored at -80° C for non-phosphopeptide analysis. LC-MS/MS measurements were performed on a QExactive (QE) Plus (peptides) and HF-X (phosphopeptides) mass spectrometer coupled to an EasyLC 1000 and EasyLC 1200 nano-flow-HPLC, respectively (all Thermo Scientific). Peptides were fractionated on a fused silica HPLC-column tip (I.D. 75 μ m, New Objective, self-packed with ReproSil-Pur 120 C18-AQ, 1.9 μ m [Dr. Maisch] to a length of 20 cm) using a gradient of A (0.1% formic acid in water) and B (0.1% formic acid in 80% acetonitrile in water). Mass spectrometers were operated in the data-dependent mode; after each MS scan (mass range $m/z = 370 - 1750$; resolution: 70'000 for QE Plus and 120'000 for HF-X) a maximum of ten, or twelve MS/MS scans were performed using a normalized collision energy of 25%, a target value of 1'000 (QE Plus) or 5'000 (HF-X), and a resolution of 17'500 for QE Plus and 30'000 for HF-X. MS raw files were analyzed using MaxQuant (version 1.6.2.10) (Cox and Mann, 2008) using a UniProt full-length *S. cerevisiae* database (March, 2016) and common contaminants, such as keratins and enzymes used for in-gel digestion, as reference. Carbamidomethylcysteine was set as fixed modification and protein amino-terminal acetylation, serine-, threonine- and tyrosine- phosphorylation, and oxidation of methionine were set as variable modifications. The MS/MS tolerance was set to 20 ppm and three missed cleavages were allowed using trypsin/P as enzyme specificity. Peptide, site, and protein FDR based on a forward-reverse database were set to 0.01, minimum peptide length was set to 7, the minimum score for modified peptides was 40, and minimum number of peptides for identification of proteins was set to one, which must be unique. MaxQuant results were analyzed using Perseus (Tyanova et al., 2016). Motif Analysis tool (NIH) was used to predict Gcn2 phosphorylation site motif. MS data have been deposited to the ProteomeXchange Consortium via the PRIDE partner repository with the dataset identifier PXD021109 (Perez-Riverol et al., 2019).

Protein purification

For Gcn2 purification, transformants of strain HQY346 bearing plasmids pDH103, pDH109 or pLD4074 were pre-cultured in synthetic dextrose medium lacking uracil and tryptophan, washed twice with sterile water, and suspended to OD₆₀₀ of 0.4 in synthetic galac-

tose medium lacking uracil, tryptophan and histidine. At OD₆₀₀ of 0.9, 10 mM 3-amino-1,2,4-triazole (3-AT) was added, and cells were further cultivated up to OD₆₀₀ of 3.0. Cells were then harvested by filtration, washed with cold distilled water containing 1 × complete EDTA-free protease inhibitor cocktail (PIC; Roche) and 1 × Pefabloc (Sigma-Aldrich), and disrupted with glass beads using a Fast-Prep-24TM (MP Biomedicals) in binding buffer (100 mM sodium phosphate [pH 8.0], 500 mM NaCl, 0.1% Triton X-100, 1 × PIC, and 1 × Pefabloc). The lysates were then clarified by centrifugation (3'220 × *g* for 5 min at 4°C) and Gcn2 was purified using anti-FLAG M2 magnetic beads (Sigma-Aldrich). After 3 h of binding at 4°C, the beads were washed with binding buffer three times, resuspended in 20 mM Tris-HCl (pH 8), 50 mM NaCl, 1 mM DTT, 1 × PIC, and 1 × Pefabloc, and used in the *in vitro* kinase assay. The polyhistidine- and GST-fusion proteins were purified from *E. coli* under non-denaturing conditions using magnetic Ni-charged MagBeads or Glutathione MagBeads (GenScript), respectively, according to manufacturer's instructions. Purified proteins were always dialyzed against the corresponding assay buffer using a Side-A-Lyzer 10K MWCO MINI dialysis device (Thermo Scientific).

In vitro Gcn2 kinase assay

12 μL of Gcn2, Gcn2^{F842L} or Gcn2-kinase-dead bound to the magnetic beads were mixed with 4 μg of recombinant substrate (i.e., His₆-Gcn20, His₆-Sui2, or His₆-Sui3; purified from *E. coli*) in kinase assay buffer (20 mM Tris-HCl [pH 8], 50 mM NaCl, 1 mM DTT, 1 × PIC, and 1 × Pefabloc). The reaction (25 μL) was started by addition of 10 μCi [γ -³²P]ATP, 100 μM cold ATP and 10 mM MgCl₂, and the samples were incubated for 15 min at 30°C. The reaction was stopped by adding Laemmli SDS-PAGE sample buffer and incubating for 10 min at 65°C. The samples were resolved by 10% SDS-PAGE, the gel was stained with Sypro Ruby (Sigma-Aldrich), dried, and subjected to autoradiography. In parallel, the assay was performed with non-radioactive ATP (1 mM) and the samples were analyzed by MS as described (Hu et al., 2019). Kinase assays with human GCN2 (GST-tagged recombinant enzyme expressed in Sf21 insect cells; Millipore) were performed with 100 ng enzyme in assay buffer (20 mM Tris-HCl [pH 8.5], 100 mM NaCl, 200 μM EDTA, 0.1% Tween-20, and 100 μM PMSF). The reaction (25 μL) was started by addition of 10 μCi [γ -³²P]ATP, 100 μM cold ATP and 10 mM magnesium acetate, the samples were incubated for 10 min at 30°C and processed as described above. The K_m values were calculated with the Prism 8 software (Graphpad) using a nonlinear regression for Michaelis-Menten enzyme kinetics and interpolation from a standard curve in a confidence interval of 95%.

Co-immunoprecipitation and immunoblot analyses

Yeast strains were grown to mid-log phase in SD-His medium, treated, or not, with 20 mM 3-AT for 30 min, collected by filtration, and frozen in liquid nitrogen. Cells were disrupted in lysis buffer (50 mM Tris-HCl [pH 7.5], 150 mM NaCl, 50 mM NaF, 5 mM EDTA, 0.1% NP-40, 60 mM β-glycerophosphate, 1 × PIC, and 1 × Pefabloc) using a FastPrep-24TM, and the lysates were then clarified by centrifugation (3'220 × *g* for 5 min at 4°C). Co-immunoprecipitation was performed with 10 mg of total protein using PierceTM Anti-HA magnetic beads (Thermo Scientific). eIF2 subunits were detected using specific rabbit antisera (Perzmaier et al., 2013). For HA-tag and c-Myc-tag detection, mouse anti-HA 12CA5 or anti-c-Myc 9E10 (Santa Cruz Biotechnology) antibodies were used, respectively. Sui2-Ser⁵² phosphorylation was monitored in whole cell lysates prepared as described (Hatakeyama and De Virgilio, 2019) using phospho-EIF2S1 (Ser⁵²) polyclonal antibody (Invitrogen). The list of primary and secondary antibodies with indicated working dilutions can be found in the [Key resources table](#). ECL Western Blotting Detection (GE Healthcare) or Radiance Plus Sensitive ECL (Azure Biosystems) were used for the western blot development. The blots were quantified using ImageJ (NIH).

β-Galactosidase assays

Yeast strains carrying p180 (*GCN4-LacZ* (Hinnebusch, 1985)), p367 (*HIS4-AUG-LacZ*) or p391 (*his4-UUG-LacZ* (Donahue and Cigan, 1988)) were grown in synthetic complete medium lacking uracil and histidine. *GCN4*-derepressing conditions were imposed by treatment with 40 mM 3-AT or 200 ng mL⁻¹ rapamycin for 4 h. Cell pellets were resuspended in Z-buffer and processed for β-galactosidase assay with the SDS/chloroform cell permeabilization method as previously described (Guarente, 1983). β-galactosidase activity was measured using 2-nitrophenyl-β-D-galactopyranoside as substrate.

Polysome profile analysis

Yeast cultures (200 mL) were grown in YPD at 30°C to OD₆₀₀ of 0.6 and treated, or not, with 200 ng mL⁻¹ rapamycin for 30 min. For the polysome analyses with strains expressing Gcn2^{F842L} (Figures 3H and 4F), strains were grown exponentially in SD-Ura at 30°C to OD₆₀₀ of 0.6. Cycloheximide was added to a final concentration of 0.1 mg mL⁻¹, and the cultures were immediately placed on ice and shaken for 5 min. Cells were harvested by centrifugation, washed with 20 mL of ice-cold breaking buffer (10 mM Tris-HCl [pH 7.5], 100 mM NaCl, 30 mM MgCl₂, and 0.1 mg mL⁻¹ cycloheximide), and resuspended in 0.8 mL breaking buffer. Glass beads were added to about one-fourth of the total volume and vortexed 8 times for 30 s with 30 s intervals on ice. The extracts were clarified by centrifugation (12'000 × *g* for 10 min at 4°C). Eight A₂₆₀ units were layered onto 10%–50% sucrose gradients containing 50 mM Tris-acetate (pH 7.5), 50 mM NH₄Cl, and 12 mM MgCl₂, which were then centrifuged at 39'000 rpm in a Sorvall TH-641 rotor at 6°C for 2 h 45 min. Sucrose gradients were analyzed using an ISCO UA-6 system with continuous monitoring at A₂₅₄.

Fluorescence spectroscopy

Fluorescence spectroscopy was used to quantify affinities of protein-protein and protein-peptide interactions by fluorescence (de) quenching. GST-EF3L (Gcn1¹³³¹⁻¹⁶⁷⁰) labeling by Alexa Fluor 488 5-TFP (Life Technologies) was performed as described

previously (Janovič et al., 2019). Measurements of EF3L interactions with Gcn20 variants were performed at room temperature in phosphate-buffered saline (pH 7.4) on a FluoroMax-4 spectrofluorometer (Horiba), monitoring fluorescence intensity at an excitation wavelength of 489 nm and an emission wavelength of 515 nm. The slit width was 10 nm and the integration time was 1 s. Peptides PTDDIAEALGELSLKKKKKKTK and PTDDIAEALGEL[pSer]LKKKKKKTK corresponding to Sui3⁶⁸⁻⁸⁹ were N-terminally conjugated with fluorescein isothiocyanate over 6-aminohexanoic acid (GenScript), and tested for GST-Tif5 and GST-Gcd6 binding at room temperature in assay buffer (30 mM HEPES [pH = 7.5], 100 mM KCl, 0.1 mM MgCl₂, 10% glycerol, 1 mM DTT, 0.1 mM PMSF, 0.5 × PhosSTOP) on a Cytation 5 plate reader (BioTek), monitoring fluorescence intensity at an excitation wavelength of 485 nm and an emission wavelength of 528 nm. Kds were calculated by Prism 8 software (Graphpad) using nonlinear asymmetric sigmoidal regression (5PL). The experiments were performed in triplicates.

QUANTIFICATION AND STATISTICAL ANALYSIS

Statistical parameters are reported in the Figures and Figure Legends.